1 **Title**

2 Type I interferon responses contribute to immune protection against mycobacterial infection

3 **Authors**

4 Andrea Szydlo-Shein[1], Blanca Sanz-Magallón Duque de Estrada[1], Joshua Rosenheim[1], Carolin T.
5 Turner[1], Aneesh Chandran[2], Evdokia Tsaliki[1], Marc C. I. Lipman[3,4], Heinke Kunst[5], Gabriele Pollara[1],
6 Philip M. Elks[6], Jean-Pierre Levraud[7], Elspeth M. Payne[8], Mahdad Noursadeghi[1], Gillian S.
7 Tomlinson[1,9]*

8 **Affiliations**

9 [1]Division of Infection and Immunity, University College London, London, UK

10 [2]Institute of Dentistry, Queen Mary University of London, London, UK

11 [3]Respiratory Medicine, Royal Free London NHS Foundation Trust, London, UK

12 [4]UCL Respiratory, University College London, London, UK

13 [5]Blizard Institute, Barts and The London School of Medicine and Dentistry, Queen Mary University
14 of London, London, UK

15 [6]The Bateson Centre, School of Medicine and Population Health, The University of Sheffield,
16 Sheffield, UK

17 [7]Université Paris-Saclay, CNRS UMR9197, Institut Pasteur, Université Paris-Cité, Institut des
18 Neurosciences Paris-Saclay, 91400 Saclay, France

19 [8]Research Department of Haematology, Cancer Institute, University College London, London, UK

20 [9]Clinical Medicine, School of Medicine and Population Health, The University of Sheffield, Sheffield,
21 UK

22 *Corresponding author

23 **Corresponding author**

24 Gillian S. Tomlinson, Email: g.tomlinson@ucl.ac.uk

ABSTRACT

Type I interferon responses have been considered detrimental to host protection in tuberculosis (TB). We provide novel data to challenge this paradigm, derived from transcriptional profiling of human in vivo immune responses to discover associations with radiographic disease severity in pulmonary TB, combined with mechanistic studies to test causality for observed associations using a zebrafish larval mycobacterial infection model. Type I interferon activity in tissue samples from the site of a standardised mycobacterial challenge, the tuberculin skin test, was associated with less severe human TB disease. Abrogation of type I interferon signalling, by CRISPR-mediated mutagenesis of *stat2*, led to increased burden and dissemination of *Mycobacterium marinum* infection in zebrafish larvae. The mechanism for increased severity of mycobacterial infection in zebrafish involves reduced recruitment of myeloid cells required to restrict bacterial growth. Our data support a clear host protective role for type I interferon responses in mycobacterial infection, with potential applications for risk-stratification of adverse outcomes and development of a host-directed therapy to mitigate against severe disease.

KEYWORDS

Tuberculosis, mycobacterial infection, zebrafish, immune response, type I interferon, macrophage, neutrophil, host-directed therapy

43 **INTRODUCTION**

44 *Mycobacterium tuberculosis* (Mtb) infection results in diverse clinical manifestations, ranging from
45 asymptomatic infection to active tuberculosis (TB), which comprises an enormous spectrum of
46 disease severity [1,2]. Although we know that immune responses contribute to the risk of disease,
47 current understanding of the role of immune response variation in disease severity is limited.
48 Identification of immune correlates of disease severity may offer new insights into the immune
49 pathways that contribute to protection and pathogenesis. This is necessary to enable novel vaccine
50 design and evaluation, stratify disease risk in people who become infected and inform development
51 of novel host-directed therapies to shorten treatment regimens, mitigate against antimicrobial
52 resistance, and against the chronic sequelae of tissue injury in TB [3].

53 To date, protective immunity has focussed on tumour necrosis factor (TNF) and type II interferon
54 mediated immune signalling pathways [4]. Type I interferon immune responses are also pervasive in
55 TB. Unlike the protective role of type I interferons in viral infections, the prevailing view has been that
56 this pathway may contribute to TB pathogenesis [5]. However, causal inferences have been limited to
57 mouse models which do not represent a natural host-pathogen interaction [6]. We sought to re-
58 evaluate the differential role of immune signalling pathways in protection or pathogenesis in TB, by
59 combining observational human data with genetic perturbation of immune signalling pathways in
60 zebrafish infected with its natural pathogen *Mycobacterium marinum* (Mm).

61 Observational immunology in human TB is limited by reverse causality. This is particularly true for
62 positive correlations between immune responses and disease severity. Therefore, we specifically
63 sought to identify negative correlations with disease severity, that are less susceptible to this
64 limitation and suggestive of protective immunity. Transcriptional profiling can be used to make
65 unbiased system level assessment of immune signalling pathways. In patients with TB, we used
66 transcriptional profiling to investigate steady state perturbation of the immune system in peripheral
67 blood [7], and to measure inducible immune responses at the tissue site of a standardised Mtb
68 challenge modelled by the tuberculin skin test (TST) [8,9]. Our innovative strategy revealed an inverse
69 relationship between type I interferon activity in the TST transcriptome and radiographic severity of
70 human TB, challenging the paradigm of a host-pathogenic role for type I interferons. Here, we

71 confirmed a role for type I interferon responses in host protection against mycobacteria by showing
72 that mutagenesis of *stat2* to abrogate downstream type I interferon signalling, led to increased
73 severity of *M. marinum* infection in zebrafish larvae, due to reduced recruitment of macrophages and
74 neutrophils required to contain bacterial growth.

75 **RESULTS**

76 **Immune pathways negatively correlated with TB disease severity are not evident in the steady**
77 **state peripheral blood transcriptome**

78 Our analysis of human immune responses in TB leveraged a previously reported cohort of patients
79 with pulmonary TB [10] which we have extended to a total sample size of 51 people with
80 microbiologically confirmed disease, within one month of commencing anti-tuberculous
81 chemotherapy (Table 1, Figure S1). We evaluated disease severity using a published radiographic
82 scoring system which incorporates extent of disease and the presence of cavitation on chest x-ray [11].
83 We performed genome-wide transcriptional profiling of peripheral blood, and punch biopsies from
84 the site of a 48 hour TST. Transcriptional changes associated with the immune response to TB were
85 identified by comparison with reference healthy control blood samples and punch biopsies from the
86 site of control saline injections. We used outlier profile analysis [12] to capture inter-individual variation
87 in immune perturbation associated with active TB. This overcomes the limitation of conventional
88 differential gene expression analysis that may exclude changes that occur in only a subset of cases.
89 In outlier profile analysis, we identified transcripts in the peripheral blood of each individual that were
90 significantly enriched (more abundant) compared to control blood samples from healthy volunteers.
91 The integrated list of outlier genes from the entire cohort defined an active TB blood transcriptome
92 comprised of 2620 genes, enriched for pathways involved in innate and adaptive immune responses
93 and cell cycle regulation (Figure S2).

94 Next, we sought to identify immunological pathways correlated with disease severity. We identified
95 individual genes in the blood transcriptome that showed statistically significant correlations with the
96 radiographic severity score (Figure 1A). Pathway analysis revealed no enrichment at pathway level
97 among genes negatively correlated with TB severity. There was modest enrichment for innate and

98 adaptive immune response pathways among genes positively correlated with radiographic disease
99 score (Figure 1B). Next, we subjected these genes to Ingenuity Pathway Analysis (IPA) upstream
100 regulator analysis to collate groups of co-regulated genes (Figure 1A and Figure S3A). These were
101 annotated by their upstream regulators at the level of cytokines, transmembrane receptors, kinases
102 and transcriptional regulators, representing the key components of signalling pathways which
103 mediate immune responses. To provide increased confidence that these modules represented co-
104 regulated genes in each molecular pathway, we retained only those that had significantly greater co-
105 correlated expression than modules of genes randomly selected from our blood transcriptomes [13].
106 Only six gene modules were identified among genes negatively correlated with disease severity, but
107 these did not represent obvious coordinated biology (Figure S3B). Among genes positively
108 correlated with TB severity 94 gene modules were identified, reflecting pro-inflammatory cytokine
109 activity, type II interferon and T cell activation and innate immune signalling pathways (Figure S3C
110 and Figure 1C).

111 **Outlier analysis of the TST transcriptome defines inducible human in vivo immune responses**
112 **in active tuberculosis**

113 We repeated the same analysis of the dynamic response to TST challenge in the same patient
114 cohort. In this analysis, we identified transcripts in the TST of each individual that were significantly
115 enriched compared to gene expression in control data from skin biopsies at the site of saline
116 injections. The integrated list of outlier genes statistically enriched in TST samples from all 51
117 individuals compared to control saline samples defined an active TB TST transcriptome comprised
118 of 3222 transcripts. This analysis revealed that although some aspects of the TST response are
119 consistent in all people, there is also considerable variability between individuals (Figure S4A). The
120 3222 transcripts identified by this approach, were enriched for canonical pathways involved in cell
121 mediated responses, consistent with our previous description of the TST gene signature identified
122 by conventional differential gene expression analysis [9,10] (Figure S4B).

123 **Reduced type I interferon activity in the TST transcriptome is associated with increased**

124 **severity of human TB disease**

125 In contrast to the peripheral blood analysis, pathway analysis of individual genes in the TST
126 transcriptome that showed statistically significant correlations with the radiographic severity score
127 identified enrichment for cell mediated immune responses among genes negatively correlated with
128 disease severity. Statistically less significant enrichment for immune response pathways was evident
129 among genes positively correlated with TB severity (Figure 2A and Figure S5A). Subsequent IPA
130 upstream regulator analysis identified 111 modules among genes inversely correlated with
131 radiographic TB severity, suggesting they may contribute to host protection against severe disease
132 (Figure 2A-C and Figure S5B). These included transcriptional modules representing pro-
133 inflammatory cytokine activity, interferon gamma and T cell activity, consistent with existing evidence
134 predominantly supporting their protective roles in TB [4] (Figure 2B). In addition, we found enrichment
135 of multiple co-regulated gene networks attributed to type I interferon signalling, suggesting that type
136 I interferon responses may also contribute to host protection in mycobacterial infection (Figure 2B,
137 C). Interferon gamma was also predicted to regulate one of only two small putative networks within
138 genes positively correlated with disease severity; the other driven by TCL1A, an AKT kinase activator
139 that promotes cellular survival [14] (Figure S5C).

140 To validate the immunological responses predicted to be associated with disease severity by
141 upstream regulator analysis, we quantified the expression of two independently derived and largely
142 non-overlapping type I interferon inducible gene modules reflecting the specific biological activity of
143 type I interferons (Table S1) [9,10], within the TB TST transcriptome (Figure 2D). This provided
144 independent validation of the inverse relationship between type I interferon responses and
145 radiographic severity of TB (Figure 2E), suggestive of a host-protective role. By contrast, the
146 expression of the entire TST transcriptome and that of three distinct independently derived modules
147 specific for interferon gamma inducible genes [9] (Table S1) did not correlate with disease severity
148 (Figure S6A-E). There was also no relationship between peripheral blood type I IFN activity and
149 radiological severity score (Figure S6F, G).

150 ***stat2* CRISPant zebrafish larvae exhibit increased susceptibility to *M. marinum* infection**

151 The finding of numerous modules pertaining to type I interferon signalling among TST transcriptome
152 genes negatively correlated with disease severity prompted us to test the role of this pathway in
153 mycobacterial infection experimentally. Since type I interferons are primarily induced following
154 activation of innate immune recognition pathways [15], we investigated their role in the zebrafish larval
155 *M. marinum* infection model, which allows exclusive assessment of innate immunity [16]. The
156 mammalian canonical type I interferon signalling pathway is highly conserved in zebrafish [17,18]
157 (Figure 3A). First, we confirmed that intravenous *M. marinum* infection of wild type zebrafish larvae
158 induces a type I interferon response, by showing enrichment for two distinct independently derived
159 transcriptional modules reflecting type I interferon activity [13,18] (Table S1) within genome-wide
160 transcriptomic data from whole embryos after four days of mycobacterial growth (Figure 3B, C). To
161 block downstream type I interferon signalling we used CRISPR-mediated mutagenesis of *stat2*, as
162 a critical component of the principal transcription factor complex which induces expression of type I
163 interferon stimulated genes (ISG) [19–21], for which there is a single zebrafish orthologue [17] (Figure 3A).
164 Injection of three guide RNA/Cas9 ribonucleoprotein (RNP) complexes each targeting a distinct *stat2*
165 exon, into one cell stage wild type zebrafish embryos led to >90% efficient mutagenesis in CRISPant
166 embryos, confirmed by next-generation sequencing (Figure S7A and Figure S8A). We verified loss
167 of functional downstream type I interferon signalling by showing that induction of the classical ISG
168 Mxa [18,21] by injection of recombinant Interferon phi 1 protein, measured by expression of a reporter
169 *mxa:mCherry* transgene [22], was significantly attenuated in *stat2* CRISPants compared to siblings
170 injected with “scrambled” (negative control) RNPs designed to lack genomic targets (Figure S7B and
171 Figure S8B-C). *stat2* CRISPants developed normally up to five days post-fertilisation (Figure S8B).

172 There was no difference in survival of *M. marinum* infected *stat2* CRISPants and scrambled RNP
173 injected siblings within the timeframe of our experiments (Figure 3D, E). However, mycobacterial
174 burden, the number of bacterial foci and the spatial dissemination of bacteria, determined by
175 quantitation of fluorescent foci of *M. marinum*, were all significantly higher in intravenously infected
176 *stat2* CRISPants compared to control RNP injected siblings, indicative of more severe disease
177 (Figure 3D, F-H). These findings are consistent with a host protective role for type I interferons in

178 mycobacterial infection, as suggested by our observation of an inverse relationship between type I
179 interferon activity and disease severity in human TB (Figure 2).

180 **Steady state neutrophil numbers are reduced in *stat2* CRISPant zebrafish larvae**

181 Macrophages are critically important for control of *M. marinum* infection in zebrafish larvae [23–25] and
182 neutrophils may also contribute to mycobacterial killing [26,27]. Therefore, to investigate the
183 mechanisms by which *stat2* deficiency leads to worse mycobacterial infection we used transgenic
184 zebrafish lines with fluorescent immune cell lineages, *Tg(mpeg1:mCherry)* [28] and *Tg(mpx:eGFP)* [29],
185 to generate *stat2* CRISPants that have fluorescent macrophages or neutrophils, respectively. First,
186 we asked whether *stat2* disruption impacted steady state macrophage or neutrophil numbers. We
187 demonstrated by quantitative fluorescence microscopy, using integrated fluorescence as a surrogate
188 for cell number, that *stat2* deficiency did not affect baseline macrophage abundance (Figure 4A, B).
189 However, it was associated with reduced neutrophil abundance (Figure 4C, D), a phenotype also
190 reported in human STAT2 deficiency [30].

191 **Recruitment of macrophages but not neutrophils to the site of sterile injury is *stat2* dependent**

192 Type I interferons have previously been shown to influence cellular migration [15,31]. Therefore, we
193 tested macrophage and neutrophil recruitment in *stat2* CRISPants using a tailfin transection model
194 of sterile injury, most commonly used to evaluate neutrophil recruitment [29] (Figure S7C). The timing
195 of neutrophil homing to the site of sterile tail fin transection was normal in *stat2* CRISPants, with
196 maximal accumulation at six hours and dissipation of recruited cells becoming evident by 24 hours,
197 similar to that of control RNP injected embryos (Figure 5A, B and Figure S9) and in keeping with
198 previous studies [29,32]. Despite baseline neutropenia, the number of neutrophils at the wound site at
199 the point of maximal recruitment in *stat2* CRISPants exceeded that of control RNP injected embryos.
200 But by 24 hours the number of neutrophils at the injury site was significantly reduced in *stat2*
201 CRISPants, likely reflecting the attenuated increase in total neutrophil numbers in response to the
202 acute inflammatory challenge (Figure 5C, D).

203 Macrophage recruitment to the site of a sterile tail wound has previously been reported to be slower
204 than that of neutrophils [32,33]. Very few macrophages were present at the tailfin transection site by

205 one hour in either *stat2* disrupted or control transgenic larvae, but recruitment progressively
206 increased until 24 hours in both groups (Figure 6). Fewer macrophages were found in the vicinity of
207 the wound site at all time points post-injury in *stat2* CRISPant transgenic embryos compared to
208 control RNP injected siblings, the majority being located outwith the tailfin (Figure 6). Taken together
209 these data suggest that *stat2* is necessary for macrophage recruitment but non-essential for
210 neutrophil recruitment to a sterile injury site. In addition, baseline neutropenia did not impact the
211 number of cells localised to the wound at peak neutrophil recruitment.

212 **Recruitment of myeloid cells to the site of *M. marinum* infection is *stat2* dependent**

213 Next we focused on macrophage recruitment to the site of mycobacterial infection because this has
214 been reported to be crucial for control of *M. marinum* growth in zebrafish larvae [24]. We found a
215 significant reduction in the number of macrophages recruited to the site of localised hindbrain
216 *M. marinum* infection in *stat2* deficient transgenic zebrafish larvae compared to their counterparts
217 injected with scrambled RNPs (Figure S7D and Figure 7A, B). We then evaluated whether *stat2*
218 disruption affected recruitment of neutrophils to the site of mycobacterial infection. We found that in
219 contrast to their normal peak recruitment to a sterile wound, the number of neutrophils attracted to
220 the site of mycobacterial disease was significantly diminished in *stat2* CRISPants (Figure 7C, D).
221 Collectively, these results demonstrate that myeloid cell recruitment to the site of *M. marinum*
222 infection is *stat2* dependent.

223 In total, the recruitment studies suggest that *stat2* disruption leads to a broad defect in macrophage
224 recruitment to both infectious and non-infectious inflammatory foci. By contrast, *stat2* is non-essential
225 for neutrophil migration to sterile injury. The latter finding is consistent with defective migration, rather
226 than neutropenia, being the principal mechanism for reduced neutrophil numbers at the site of
227 *M. marinum* infection.

228 **DISCUSSION**

229 We have taken an innovative approach, combining molecular and systems level evaluation of human
230 immune responses to a standardised experimental challenge, to identify biological pathways
231 associated with TB disease severity. We experimentally validated host factors responsible for

differences in phenotype using a relevant, tractable animal model which represents a natural host-pathogen relationship [16]. Molecular interrogation of human in vivo responses to Mtb revealed that reduced type I interferon activity within the TST transcriptome was associated with worse pulmonary disease. Deficient type I interferon signalling, achieved by genetic disruption of *stat2*, led to more severe mycobacterial infection in zebrafish larvae, via a mechanism involving impaired recruitment of macrophages and neutrophils to the site of disease and reduced neutrophil numbers at baseline. Taken together our results demonstrate an important role for type I interferon responses in contributing to innate immune protection against mycobacterial disease.

Previous studies report peripheral blood interferon-inducible gene expression that diminishes with successful treatment in human active TB [7,34,35]. These transcriptional signatures comprise both type I and type II interferon inducible genes but have mainly been interpreted as type I interferon responses, fostering the view that type I interferons are detrimental to the host in human TB. In the present study we found no relationship between disease severity and peripheral blood expression of gene modules specific for type I interferon activity. Mouse data predominantly suggest that type I interferon responses contribute to increased susceptibility to mycobacterial infection, by mechanisms including antagonism of IL1 mediated protection [36–38] and reduced responsiveness of macrophages to interferon gamma [39]. However, this phenotype has not been universally observed, likely due to differences in host and pathogen genetics [5]. Moreover, impaired type I interferon responses are generally associated with relatively minor differences in bacterial burden or survival [5]. Of note, Mtb is not a natural mouse pathogen, and this approach may not model host-pathogen interactions in human TB faithfully [6].

In support of a protective role for type I interferons, adjunctive interferon alpha therapy in addition to conventional anti-tuberculous antibiotic treatment led to symptomatic and radiological improvement, with a reduction in bacterial burden in respiratory tract samples, in small-scale human studies [40–42]. In keeping with this, an early peripheral blood type I interferon-inducible gene signature predicts successful BCG-induced protection of macaques from subsequent Mtb challenge [43]. Type I interferon mediated restriction of mycobacterial growth in in vitro granulomas comprising collagen impregnated microspheres containing Mtb infected human peripheral blood mononuclear cells

260 (PBMC) [44] also suggests that type I interferon responses benefit the host.

261 Our observation of reduced recruitment of macrophages to the site of disease is likely the most
262 important factor driving increased susceptibility to *M. marinum* infection in *stat2* CRISPants.
263 Although macrophages have been implicated in the dissemination of *M. marinum* in zebrafish larvae
264 [23,45], reduction of total macrophage numbers, impaired macrophage migration to the site of
265 mycobacterial infection or failure to control intracellular bacterial growth within macrophages have
266 all been associated with poor outcome [23–25,46,47]. In contrast, increasing macrophage numbers via
267 augmentation of M-CSF signalling either pre- or post-granuloma formation, promotes resistance to
268 *M. marinum* infection by reducing granuloma necrosis, with consequent curtailment of extracellular
269 mycobacterial growth [24]. The recent report that human genetically inherited CCR2 deficiency is
270 associated with reduced pulmonary recruitment of monocytes, resulting in depleted numbers of
271 functionally normal alveolar macrophages and increased susceptibility to mycobacteria, is also
272 consistent with the concept that adequate numbers of macrophages at the site of infection are
273 important for protective anti-mycobacterial immunity [48].

274 The reduction in neutrophils present at the site of *M. marinum* infection in *stat2* CRISPants may have
275 arisen due to baseline neutropenia, defective migration or both combined. On the basis that steady
276 state neutropenia did not affect the timing and magnitude of peak neutrophil recruitment to sterile
277 injury, impaired migration is probably the main driver of this phenotype, which likely also contributed
278 to increased severity of mycobacterial disease. Previous data show that reduced access of
279 neutrophils to mycobacteria leads to increased bacterial burden in a zebrafish line in which
280 neutrophils express mutant *cxcr4*, resulting in peripheral neutropenia and impaired neutrophil
281 recruitment to sites of inflammation, due to their retention in haematopoietic tissue [26,49].

282 Our study has some limitations. We were not able to address the reasons for variation in type I
283 interferon activity in our human cohort. Variation in type I interferon responses may arise due to
284 genetically or epigenetically encoded variation in the immune response to Mtb, neutralising type I
285 interferon auto-antibodies, burden and virulence of the mycobacterial inoculum and stochasticity in
286 the immune response pathway following exposure [50–54]. Our sample size is insufficient for robust
287 detection of associations between genetic variation and the expression levels of type I interferon

288 signalling pathway genes. Serum samples for measurement of autoantibodies to type I interferons
289 are not available, although anti-interferon antibodies are very rare in cohorts of this age
290 distribution [55]. We were also unable to completely disentangle whether reduced neutrophil
291 recruitment to the site of *M. marinum* infection was a consequence of neutropenia or impaired
292 migration. We have not determined the mechanism by which attenuated type I interferon signalling
293 leads to reduced myeloid cell recruitment to *M. marinum*. The expression of several chemokines is
294 type I interferon inducible [31,56,57] and the CCR2-CCL2 and CXCR3-CXCL11 chemokine axes are
295 known to be involved in macrophage recruitment to *M. marinum* [45,58]. Future studies are required to
296 test the hypothesis that *stat2* mutagenesis disrupts chemokine-mediated cellular recruitment to the
297 site of mycobacterial disease. Nonetheless, our work provides new insights into type I interferon
298 mediated host protection against mycobacterial infection.

299 Our findings have potential implications for risk stratification of individuals in whom any of the above
300 mechanisms predisposing to low type I interferon activity are identified. In active TB, such individuals
301 could be targeted for longer or more intensive drug regimens, or adjunctive type I interferon therapy
302 delivered to the respiratory tract, to mitigate against severe disease. Early intervention with type I
303 interferon treatment, before destruction of the lung parenchyma, is likely to be crucial to augment
304 macrophage containment of Mtb, but timing and duration of therapy will require evaluation in
305 relatively large-scale experimental medicine trials.

306 METHODS

307 Ethics statement

308 The study was approved by the London Bloomsbury Research Ethics Committee (16/LO/0776).
309 Written informed consent was obtained from all participants.

310 Study design

311 We aimed to identify human immune pathways that correlate with severity of TB disease, using
312 transcriptional profiling of biopsies from the TST as a surrogate for immune responses to Mtb in the
313 lung, and peripheral blood samples. We tested causation for observed associations by genetic
314 manipulation of identified pathways in the zebrafish larval mycobacterial infection model. To

315 encompass a broad spectrum of disease severity we recruited 51 adults (>18 years) from four
316 London hospitals, newly diagnosed with smear or culture positive pulmonary TB, who were within
317 four weeks of starting treatment. This is in keeping with the median sample size of previous studies
318 which have successfully demonstrated a relationship between severity of TB disease and
319 immunological parameters [7,59–62]. Individuals with coincident human immunodeficiency virus
320 infection, malignancy, taking immunomodulatory therapy, a history of immunization within the
321 preceding two weeks or previous keloid formation, or unable to give informed consent were
322 excluded. Study participants underwent blood collection into Tempus tubes before intradermal
323 injection of 0.1 ml of two units of tuberculin (AJ Vaccines) or saline in the volar aspect of the forearm
324 as previously described [8–10]. At 48 hours clinical induration at the injection site was measured,
325 immediately prior to sampling by 3mm punch biopsy as previously described [8,9]. Additional saline
326 samples from individuals with cured or latent TB, BCG vaccine recipients and healthy volunteers
327 have been described previously [10]. Control blood samples from healthy individuals have been
328 described previously [13].

329 **RNA purification from blood, skin biopsy and zebrafish embryo samples**

330 Total blood RNA was extracted using the Tempus Spin RNA Isolation Kit (Ambion; Life
331 Technologies). Globin mRNA was removed using the GlobinClear kit (Life Technologies). Skin
332 biopsies were homogenized as previously described [10]. Pooled zebrafish embryos (25-30 per
333 experimental condition) collected in Qiazol (Qiagen) were homogenized in CK14 lysing kit tubes
334 (Bertin Instruments) using a Precellys Evolution homogenizer (Bertin Instruments) for 10-20 seconds
335 at 5500 rpm. Total RNA from skin biopsies and zebrafish samples was purified using the RNEasy
336 mini and micro kits (Qiagen), respectively, according to the manufacturer's instructions. Genomic
337 DNA was removed using the TURBO DNA-free kit (ThermoFisher).

338 **Transcriptional profiling of blood, skin biopsy and zebrafish larval samples**

339 Genome-wide mRNA sequencing was performed as previously described [10,63]. Complementary DNA
340 (cDNA) libraries were prepared using the KAPA HyperPrep kit (Roche). Sequencing was performed
341 in paired-end mode with the NextSeq 500 High Output 75 Cycle Kit (Illumina) using the NextSeq500

342 system (Illumina) according to the manufacturer's instructions, generating a median of 24 million
343 (range 14.7-32.4 million) 41 base pair reads per human blood sample, 22 million (range 12.3-27.9
344 million) reads per human TST sample and 16.8 million (range 15.1-18.1 million) reads per zebrafish
345 sample. Transcript alignment and quantitation against the Ensembl GRCh38 human genome
346 assembly release 100 or GRCz11 zebrafish genome assembly release 104 was performed using
347 Kallisto [64]. Transcript-level output counts and transcripts per million (TPM) values were summed on
348 gene level and annotated with Ensembl gene ID, gene name, and gene biotype using the
349 R/Bioconductor packages tximport and BiomaRt [65,66]. Downstream analysis was performed using R
350 3.6.3 on log2 transformed TPM values for protein-coding genes only. 0.001 was added to all TPM
351 values prior to log2 transformation. To determine the need for and effect of batch correction in the
352 human data, principal component analysis (PCA) was performed using the prcomp R function on the
353 integrated list of genes with the 10% lowest variance in expression for each library preparation date.
354 This revealed separation of three TST samples in PC1, likely accounted for by lower RNA
355 concentrations or RIN values compared to the rest of the dataset (Figure S1A). After batch correction
356 performed using the ComBat function of the sva R package [67], allocating samples with PC1 score
357 <0 and >0 to separate batches, this was no longer evident (Figure S1B).

358 **Radiographic quantitation of TB severity**

359 Disease severity was evaluated by estimating the extent of radiographic abnormalities and whether
360 cavitation was present on chest x-ray at the time of diagnosis, as previously described [10,11].

361 **Outlier analysis**

362 The BioBase Bioconductor R package was used to perform outlier analysis based on the z-score
363 outlier detection (ZODET) algorithm [12], to identify transcripts in each TB patient blood sample whose
364 expression was significantly higher than the mean expression in control blood samples from healthy
365 volunteers [13] and transcripts in each TST sample whose expression was significantly higher than the
366 mean expression in control saline samples (>2SD, p value <0.05), with a fold difference filter of >1
367 log2. Chi-squared tests implemented in R were then used to identify outlier genes statistically
368 enriched in blood samples from TB patients compared to healthy individuals and TST samples

369 compared to saline samples, using a p value <0.05. To avoid type 2 error no correction for multiple
370 testing was used in this analysis. In instances where multiple Ensembl gene IDs were associated
371 with a single gene symbol, duplicate gene symbols were removed to retain the replicate with the
372 highest expression for each sample.

373 **Pathway enrichment analysis**

374 The biological pathways represented by the entire blood and TST transcriptomes and genes in each
375 transcriptome positively and negatively correlated with radiographic severity score (Spearman rank
376 correlation p value <0.05, without correction for multiple testing, to prevent type 2 error) were
377 identified by Reactome pathway enrichment analysis using XGR as previously described [68,69]. For
378 visualization, 15 pathway groups were identified by hierarchical clustering of Jaccard indices to
379 quantify similarity between the gene compositions of each pathway. For each group the pathway
380 term with the largest number of annotated genes was then selected as representative of enriched
381 biology.

382 **Upstream regulator analysis**

383 Peripheral blood and TST transcriptome genes whose expression was significantly correlated with
384 radiographic severity of TB disease were identified by Spearman rank correlation, p value <0.05,
385 without correction for multiple testing, to prevent type 2 error. Genes positively and negatively
386 correlated with disease severity were separately subjected to Ingenuity Pathway Analysis (Qiagen)
387 to identify upstream molecules responsible for their transcriptional regulation. This analysis was
388 restricted to molecules annotated with the following functions: cytokine, transmembrane receptor,
389 kinase and transcriptional regulator, representing the canonical components of pathways which
390 mediate transcriptional reprogramming in immune responses. Enriched molecules with an adjusted
391 p value <0.05 were considered statistically significant.

392 **Upstream regulator functional modules**

393 Blood and TST gene modules representing the functional activity of their upstream molecule were
394 identified as previously described [13]. In brief, we calculated the average correlation coefficient for
395 pairwise correlations of the expression levels of the target genes associated with each predicted

396 upstream regulator. We compared these to the distribution of average correlation coefficients
397 obtained from 100 iterations of randomly selecting equivalent sized groups of genes from the blood
398 or TST transcriptome. Only target gene modules with average correlation coefficients higher than
399 the mean of the distribution of equivalent sized randomly selected groups by ≥2 SD (Z score ≥2) with
400 false discovery rate <0.05, were retained. We visualised these upstream regulator modules as
401 network diagrams using the Force Atlas two algorithm in Gephi v0.9.2 [70], depicting all statistically
402 over-represented molecules (false discovery rate <0.05) predicted to be upstream of ≥4 target genes.

403 **Transcriptional modules**

404 Interferon inducible transcriptional module gene lists are provided in Table S1. Independently derived
405 human type I and type II interferon inducible gene modules were described previously [9,10,13]. Two
406 further modules were derived to distinguish type I or type II interferon inducible gene expression
407 using published transcriptional data for primary human keratinocytes stimulated with a selection of
408 cytokines (Gene Expression Omnibus accession: GSE36287) [71]. Stimulus-specific modules for type
409 I interferon (interferon alpha) and type II interferon (interferon gamma) were derived by selecting
410 genes overexpressed >4-fold in the cognate cytokine condition relative to all non-cognate conditions
411 combined (paired t test with α of p<0.05 without multiple testing correction), excluding genes also
412 induced by each non-cognate cytokine condition, using the same criteria. The babelgene R package
413 (https://igordot.github.io/babelgene/) was used to convert human gene symbols to their respective
414 zebrafish orthologues to generate the zebrafish Stat1 module, excluding zebrafish genes reported
415 to be an orthologue of more than one human gene. The zebrafish type I interferon inducible gene
416 module comprises 360 genes whose expression was significantly induced (≥2 fold, adjusted p value
417 <0.05) six hours after intravenous injection of three day post-fertilisation (dpf) larvae with 1 nl of
418 recombinant interferon phi 1 protein (1 mg/ml) as previously described [18].

419 **Venn diagrams**

420 Area-proportional Venn diagrams visualizing the overlap between constituent genes in
421 transcriptional modules were generated using BioVenn [72].

422 **Zebrafish husbandry**

423 Zebrafish were raised and maintained at 28.5°C following a 14/10 light/dark cycle according to
424 standard protocols [73] in University College London (UCL) and Neuro-PSI Zebrafish Facilities. All
425 work was approved by the British Home Office (Project License PP8780756) and the French Ministry
426 for Research and Higher Education (Project License 39238). All experiments were performed in
427 accordance with the relevant guidelines and regulations, on larvae up to five days post-fertilisation,
428 before they are protected under the Animals (Scientific Procedures) Act. Adult zebrafish were
429 spawned to collect embryos for experiments. Table S2 lists the lines used in this study [22,28,29].
430 Embryos were maintained at 28.5°C in egg water containing 60 µg/ml Tropic Marin Sea Salt
431 (Norwood Aquarium) and anaesthetised with egg water containing 200 µg/ml buffered tricaine (3-
432 aminobenzoic acid ethyl ester) (Sigma-Aldrich) during injection, tail fin transection and imaging.
433 Larvae used for in vivo imaging were maintained in egg water supplemented at 24 hours post-
434 fertilisation (hpf) with 0.003% PTU (1-phenyl-2-thiourea) (Sigma-Aldrich) to inhibit melanisation.

435 **CRISPant Generation**

436 To maximise the likelihood of loss of functional protein we employed a previously described triple-
437 exon targeting approach [74], with the modification that Cas9 protein was not diluted before use.
438 CRISPR RNA (crRNA) (Alt-R CRISPR-Cas9 crRNA), tracrRNA (Alt-R CRISPR-Cas9 tracrRNA) and
439 recombinant Cas9 protein (Alt-R Streptococcus pyogenes Cas9 Nuclease V3) were obtained from
440 Integrated DNA Technologies (IDT). Three pre-designed crRNAs targeting distinct exons were
441 selected for the *stat2* gene, prioritizing those that targeted early, asymmetric (not divisible by three)
442 exons common to both protein-coding transcripts, with low off-target and high on-target scores and
443 in a genomic position which allowed design of primers flanking the target site to generate a ~200 bp
444 amplicon, for verification of mutagenesis by next generation sequencing (MiSeq). crRNA sequences
445 and genomic locations are provided in Table S3. To generate gRNAs equal volumes of crRNA and
446 tracrRNA diluted to 61 µM in Duplex buffer (IDT) were annealed at 95°C for 5 minutes. Equal
447 volumes of gRNA (61 µM) and Cas9 protein (61 µM) were incubated at 37°C for 5 minutes to
448 assemble separate 30.5 µM ribonucleoproteins (RNPs) for each target. Equal volumes of the three
449 RNPs were pooled, prior to injection giving a final concentration of 10.2 µM for each. Negative control

450 “scrambled” crRNAs computationally designed to be non-targeting (Alt-R CRISPRCas9 Negative
451 Control crRNA #1, #2, #3) were prepared and pooled as described above. 0.5 nl of pooled *stat2*
452 RNPs or scrambled RNPs was injected into the yolk sac of single-cell stage wild type or transgenic
453 zebrafish embryos before cell inflation as previously described [74]. After injections embryos were
454 transferred into sterile petri dishes with fresh egg water and maintained at 28.5°C to the appropriate
455 age for experiments, as described below.

456 **Interferon phi 1 stimulation**

457 Three dpf *stat2* CRISPant *Tg(mxa:mCherry)* larvae and scrambled RNP injected siblings were
458 injected in the coelomic cavity with 1 nl of recombinant zebrafish interferon phi 1 protein (1.25 mg/ml),
459 produced as previously described [75]. *stat2* and control CRISPants were shuffled so that injections
460 were performed blindly. Bovine serum albumin (BSA) (1.25 mg/ml) was injected as a control.
461 Interferon phi 1 and BSA solutions were supplemented with 0.2% phenol red (Sigma-Aldrich) to
462 visualize the inoculum. Induction of Mxa reporter expression was determined by fluorescence
463 microscopy 24 hours post-injection.

464 ***M. marinum* infection**

465 *M. marinum* M strain expressing the pmsp12 mWasabi [76] or psMT3 mCherry plasmid [77] was cultured
466 using Middlebrook 7H10 agar (Becton Dickinson and Company) supplemented with 0.5% oleic
467 acid/albumin/dextrose/catalase (OADC) (Becton Dickinson and Company), 0.5% glycerol (Sigma-
468 Aldrich) and hygromycin (50 µg/ml) (Fisher Scientific). To generate bacterial suspensions for
469 injection, *M. marinum* from agar plates was cultured statically at 28.5°C for 24-36 hours in 10 ml
470 Middlebrook 7H9 broth (Becton Dickinson and Company) supplemented with 10%
471 albumin/dextrose/catalase (ADC) (Becton Dickinson and Company) and hygromycin (50 µg/ml)
472 (Fisher Scientific). Bacteria were harvested at mid-log growth (optical density (OD)600nm 0.7–1),
473 (OD)600nm 1 representing 10^8 colony forming units (cfu)/ml, washed three times in phosphate
474 buffered saline (PBS) (Gibco) and resuspended in 2% polyvinylpyrrolidone (PVP)40 (Sigma-
475 Aldrich)/PBS containing 10% phenol red (Sigma-Aldrich) to aid visualisation of injections [78].

476 Zebrafish embryos were manually dechorionated using jeweller’s forceps (Dumont #5, World

477 Precision Instruments) prior to bacterial infection. To generate systemic infection, 400 cfu
478 *M. marinum* in a volume of 1 nl were microinjected into the caudal vein of embryos staged at
479 28-30 hpf. Four days post-infection, embryos were either subjected to fluorescence microscopy to
480 measure disease severity or 25-30 per condition pooled and harvested in Qiazol (Qiagen) for
481 evaluation of immune responses by RNAseq. To generate localised infection, 200 cfu *M. marinum*
482 in a volume of 1 nl were injected into the hindbrain ventricle (HBV) of two dpf zebrafish larvae.
483 Cellular recruitment was evaluated by fluorescence microscopy at 6-18 hours post-infection.

484 **Tailfin transection**

485 Tailfin transections were performed as described previously [29,79]. Briefly, live anaesthetised three dpf
486 zebrafish larvae were transferred with a 1 ml Pasteur pipette (Scientific Laboratory Supplies) to a
487 sterile petri dish containing 2% agarose (Bioline). Transections of the caudal fin were performed
488 using a sterile microscalpel (World Precision Instruments) by applying steady downward pressure to
489 create the incision at the boundary with the notochord. Following injury, larvae were rinsed in egg
490 water and maintained in individual wells of a 96-well tissue culture plate (TPP) at 28.5°C until live
491 imaging to quantify neutrophil or macrophage recruitment to the site of injury at 1, 6 and 24 hours-
492 post-wound (hpw).

493 **Fluorescence microscopy**

494 All fluorescence microscopy was performed on live, anasethised larvae. For quantitation of bacterial
495 burden and dissemination four days post-infection, steady state neutrophil numbers at two dpf and
496 cellular recruitment at 2-4 dpf, larvae were imaged using an M205FA stereofluorescence microscope
497 (Leica) with a 1x objective. Larvae were imaged on a flat 1% agarose plate for quantitation of severity
498 of mycobacterial infection and steady state neutrophil numbers and a 96-well tissue culture plate
499 (TPP) in which the wells were coated with 1% agarose, for cellular recruitment to tailfin transection.
500 Micro-wells were created in 1% agarose using a Stampwell Larvae 1 device (Idylle) for optimal
501 positioning of 2-3 dpf larvae for imaging of cellular recruitment to hindbrain ventricle *M. marinum*
502 infection. Brightfield and fluorescence images were captured using a DFC365 FX camera (Leica)
503 and exported as 16-bit Tagged Image Format (TIF) files for analysis. For quantitation of steady state

504 macrophage numbers three dpf larvae were imaged in 96-well alignment plates (Funakoshi)
505 containing 75 µl egg water per well using a high-content wide-field fluorescence microscope
506 (Hermes, IDEA Bio-Medical) with a 4x objective, capturing five z planes 50.6 µm apart in four
507 contiguous fields of view per embryo. We created an ImageJ macro to semi-automate generation of
508 single maximum intensity projection z-stack montages from the Hermes images, which were saved
509 as 16-bit TIF files for analysis (Table S4). Mxa reporter expression was recorded with an EVOS
510 M7000 microscope (ThermoFisher) equipped with a 2x/NA0.06 objective and Texas Red
511 fluorescence cube. Larvae were positioned laterally in micro-wells created in 2% agarose with an in-
512 house-printed stamp. A single fluorescence plane was recorded as the depth of field is sufficient to
513 capture the entire larva. Transmitted light images were also recorded and both were exported as 16-
514 bit TIF files.

515 **Image analysis**

516 To quantify bacterial burden, number of bacterial foci and spatial distribution of bacteria, images
517 were analysed using custom QuantiFish software, previously developed in our group, to enable rapid
518 quantitation of fluorescent foci in zebrafish larvae [80]. Mxa reporter fluorescence was measured with
519 ImageJ. Transmitted and fluorescence images were stacked. Images were slightly rotated to
520 horizontality where necessary. A 600x100 pixel rectangular region of interest was defined on the
521 transmitted light image to encompass the entire gut and liver areas. Mean fluorescence intensity was
522 then measured on the fluorescence image. For quantitation of total cell number and recruitment of
523 fluorescent immune cells to the site of tailfin transection we developed a new custom Python script
524 which enables quantitation of integrated fluorescence within concentric zones (known as Sholl
525 circles) [81] (Figure S9). To achieve this, the script leverages the OpenCV, NumPy [82], Matplotlib, SciPy
526 (http://www.scipy.org), scikit-image [83] and pandas Python libraries to facilitate image processing and
527 data extraction (Table S5). First the user is prompted to select a folder containing images for
528 analysis, as well as the file extensions corresponding to the brightfield and fluorescence images,
529 which are essential for the subsequent steps. The script then iterates through each pair of brightfield
530 and fluorescent images prompting the user to define two points on the brightfield image, which serve
531 as the start and end positions between which to create concentric circular regions [81] on the

532 corresponding fluorescence image. The script employs the image processing techniques described
533 in Table S5 to quantify integrated fluorescence of the entire image and that within each region, as
534 surrogates for the total number of immune cells and the number at each spatial location, respectively
535 and generates output files containing this information. Integrated fluorescence within the first zone
536 (the wound site) and distance from the site of tailfin transection of the zone in which the maximal
537 integrated fluorescence (a surrogate for the highest cell numbers) was detected (identified manually)
538 were used as measures of immune cell recruitment for each zebrafish larva. The number of cells
539 recruited to the site of hindbrain *M. marinum* infection was quantified by manual counting.

540 **Genotyping by next generation sequencing**

541 ***Genomic DNA extraction***

542 Genomic DNA was extracted from anasethetised individual zebrafish larvae using the modified hot
543 sodium hydroxide and Tris (HotSHOT) method as previously described [74,84]. Briefly, larvae in 96-well
544 plates were incubated in 50 µl base solution (25 mM KOH, 0.2 mM EDTA in water) at 95°C for 30
545 min then cooled to room temperature, before addition of 50 µl neutralization solution (40 mM Tris-
546 HCL in water).

547 ***PCR***

548 Extracted DNA (2 µl per 50 µl reaction) was subjected to PCR using Phusion High-Fidelity DNA
549 Polymerase (New England Biolabs) (98°C for 30 seconds (s), once only, 40 cycles of 98°C for 10 s,
550 59°C for 30 s, 72°C for 20 s, 72°C for 10 minutes, once only). Sequences and genomic positions of
551 the primers used are provided in Table S3. Successful amplification of a single product of
552 approximately 300 bp was verified by 2% agarose (Bioline) Tris-borate-EDTA (TBE) containing
553 Redsafe (Chembio) gel electrophoresis. PCR products were purified using ExoSAP-IT Express
554 (ThermoFisher), concentration of purified DNA determined by Nanodrop spectrophotometer
555 (ThermoFisher) and samples diluted to 15-25 ng/µl for sequencing.

556 ***Next generation sequencing and data analysis***

557 Sequencing was performed by the UCL Fish Genomic Service using the MiSeq Reagent Kit v2 (300-
558 cycles) (Illumina) and the MiSeq system (Illumina) in paired end mode, according to the

559 manufacturer's instructions. Sequencing data were received as two FASTQ files (forward and
560 reverse) for each sample. Visual sequence analysis was performed using Geneious 10.2.6
561 (https://www.geneious.com) for initial verification of successful genome editing close to the PAM site.
562 Objective quantitation of the proportion of reads mutated and predicted to be frameshifted was
563 achieved using the ampliCan R package [85], which utilizes the FASTQ files and a metadata file
564 providing the amplicon, protospacer adjacent motif (PAM) and primer sequences (Table S3) and
565 sample information, as previously described [74]. AmpliCan was run with default parameters, with the
566 exception that min_freq = 0.005 (mutations at a frequency below this threshold were considered a
567 sequencing error) and average_quality = 25. Mutations present in uninjected or scrambled RNP
568 injected control samples were not included as Cas9 induced mutations.

569 **Statistical analysis**

570 Statistical analysis was performed using GraphPad Prism 9.3.1 for Windows (GraphPad Software)
571 and R3.6.3. Chi-squared tests were used to identify outlier genes statistically enriched in
572 transcriptomic data from blood samples from people with TB compared to healthy individuals and
573 TST samples compared to saline samples, with no correction for multiple testing to avoid type 2
574 error. Spearman rank correlation was used to determine the strength of relationship between blood
575 and TST transcriptome gene expression and TB disease severity (two-tailed), transcript levels of
576 upstream regulator target gene modules, blood and TST random gene modules (one-tailed, positive
577 correlation only) and mean expression of transcriptional modules in blood and TST transcriptomic
578 data with severity of TB disease (two-tailed). The Benjamini-Hochberg correction method for multiple
579 comparisons was used to identify upstream regulator target gene modules with average correlation
580 coefficients significantly higher than the mean of the distribution of equivalent sized randomly
581 selected gene modules by ≥2 SD (Z score ≥2) with false discovery rate <0.05. Survival of *stat2*
582 CRISPant and control zebrafish larvae was compared using a log-rank (Mantel-Cox) test; a p value
583 <0.05 was considered significant. On scatter plots horizontal lines represent median values and error
584 bars indicate the interquartile range. On box and whisker plots horizontal lines represent median
585 values, box limits indicate the interquartile range and whiskers extend between the 5th and 95th
586 percentiles of the data. Two-tailed Mann-Whitney tests were used for two group comparisons of

587 unpaired data; a p value <0.05 was considered significant. Where p values are not presented on
588 graphs, * denotes p<0.05.

589 **REFERENCES**

590 1. Coussens, A.K., Zaidi, S.M.A., Allwood, B.W., Dewan, P.K., Gray, G., Kohli, M., Kredo, T.,
591 Marais, B.J., Marks, G.B., Martinez, L., et al. (2024). Classification of early tuberculosis states
592 to guide research for improved care and prevention: an international Delphi consensus exercise.
593 Lancet Respir. Med. *12*, 484–498. https://doi.org/10.1016/S2213-2600(24)00028-6.

594 2. Cadena, A.M., Fortune, S.M., and Flynn, J.L. (2017). Heterogeneity in tuberculosis. Nat. Rev.
595 Immunol. *17*, 691–702. https://doi.org/10.1038/nri.2017.69.

596 3. Kaufmann, S.H.E., Lange, C., Rao, M., Balaji, K.N., Lotze, M., Schito, M., Zumla, A.I., and
597 Maeurer, M. (2014). Progress in tuberculosis vaccine development and host-directed therapies-
598 -a state of the art review. Lancet Respir. Med. *2*, 301–320. https://doi.org/10.1016/S2213-
599 2600(14)70033-5.

600 4. Kinsella, R.L., Zhu, D.X., Harrison, G.A., Mayer Bridwell, A.E., Prusa, J., Chavez, S.M., and
601 Stallings, C.L. (2021). Perspectives and Advances in the Understanding of Tuberculosis. Annu.
602 Rev. Pathol. Mech. Dis. *16*, 377–408. https://doi.org/10.1146/annurev-pathol-042120-032916.

603 5. Moreira-Teixeira, L., Mayer-Barber, K., Sher, A., and O'Garra, A. (2018). Type I interferons in
604 tuberculosis: Foe and occasionally friend. J. Exp. Med. *215*, 1273–1285.
605 https://doi.org/10.1084/jem.20180325.

606 6. Kramnik, I., and Beamer, G. (2016). Mouse models of human TB pathology: roles in the analysis
607 of necrosis and the development of host-directed therapies. Semin. Immunopathol. *38*, 221–237.
608 https://doi.org/10.1007/s00281-015-0538-9.

609 7. Berry, M.P.R., Graham, C.M., McNab, F.W., Xu, Z., Bloch, S.A.A., Oni, T., Wilkinson, K.A.,
610 Banchereau, R., Skinner, J., Wilkinson, R.J., et al. (2010). An interferon-inducible neutrophil-
611 driven blood transcriptional signature in human tuberculosis. Nature *466*, 973–977.
612 https://doi.org/10.1038/nature09247.

613 8. Tomlinson, G.S., Cashmore, T.J., Elkington, P.T.G., Yates, J., Lehloenya, R.J., Tsang, J.,
614 Brown, M., Miller, R.F., Dheda, K., Katz, D.R., et al. (2011). Transcriptional profiling of innate
615 and adaptive human immune responses to mycobacteria in the tuberculin skin test. Eur. J.
616 Immunol. *41*, 3253–3260. https://doi.org/10.1002/eji.201141841.

617 9. Bell, L.C.K., Pollara, G., Pascoe, M., Tomlinson, G.S., Lehloenya, R.J., Roe, J., Meldau, R.,
618 Miller, R.F., Ramsay, A., Chain, B.M., et al. (2016). In Vivo Molecular Dissection of the Effects
619 of HIV-1 in Active Tuberculosis. PLoS Pathog. *12*, e1005469.
620 https://doi.org/10.1371/journal.ppat.1005469.

621 10. Pollara, G., Turner, C.T., Rosenheim, J., Chandran, A., Bell, L.C.K., Khan, A., Patel, A., Peralta,
622 L.F., Folino, A., Akarca, A., et al. (2021). Exaggerated IL-17A activity in human in vivo recall
623 responses discriminates active tuberculosis from latent infection and cured disease. Sci. Transl.
624 Med. *13*, eabg7673. https://doi.org/10.1126/scitranslmed.abg7673.

625 11. Ralph, A.P., Ardian, M., Wiguna, A., Maguire, G.P., Becker, N.G., Drogumuller, G., Wilks, M.J.,
626 Waramori, G., Tjitra, E., Sandjaja, null, et al. (2010). A simple, valid, numerical score for grading
627 chest x-ray severity in adult smear-positive pulmonary tuberculosis. Thorax *65*, 863–869.
628 https://doi.org/10.1136/thx.2010.136242.

629 12. Roden, D.L., Sewell, G.W., Lobley, A., Levine, A.P., Smith, A.M., and Segal, A.W. (2014).
630 ZODET: software for the identification, analysis and visualisation of outlier genes in microarray
631 expression data. PloS One *9*, e81123. https://doi.org/10.1371/journal.pone.0081123.

632 13. Chandran, A., Rosenheim, J., Nageswaran, G., Swadling, L., Pollara, G., Gupta, R.K., Burton,
633 A.R., Guerra-Assunção, J.A., Woolston, A., Ronel, T., et al. (2022). Rapid synchronous type 1
634 IFN and virus-specific T cell responses characterize first wave non-severe SARS-CoV-2
635 infections. Cell Rep. Med. *3*, 100557. https://doi.org/10.1016/j.xcrm.2022.100557.

636 14. Paduano, F., Gaudio, E., Mensah, A.A., Pinton, S., Bertoni, F., and Trapasso, F. (2018). T-Cell
637 Leukemia/Lymphoma 1 (TCL1): An Oncogene Regulating Multiple Signaling Pathways. Front.
638 Oncol. *8*, 317. https://doi.org/10.3389/fonc.2018.00317.

639 15. McNab, F., Mayer-Barber, K., Sher, A., Wack, A., and O'Garra, A. (2015). Type I interferons in
640 infectious disease. Nat. Rev. Immunol. *15*, 87–103. https://doi.org/10.1038/nri3787.

641 16. Ramakrishnan, L. (2013). The zebrafish guide to tuberculosis immunity and treatment. Cold
642 Spring Harb. Symp. Quant. Biol. *78*, 179–192. https://doi.org/10.1101/sqb.2013.78.023283.

643 17. Langevin, C., Aleksejeva, E., Passoni, G., Palha, N., Levraud, J.-P., and Boudinot, P. (2013).
644 The antiviral innate immune response in fish: evolution and conservation of the IFN system. J.
645 Mol. Biol. *425*, 4904–4920. https://doi.org/10.1016/j.jmb.2013.09.033.

646 18. Levraud, J.-P., Jouneau, L., Briolat, V., Laghi, V., and Boudinot, P. (2019). IFN-Stimulated
647 Genes in Zebrafish and Humans Define an Ancient Arsenal of Antiviral Immunity. J. Immunol.
648 Baltim. Md 1950 *203*, 3361–3373. https://doi.org/10.4049/jimmunol.1900804.

649 19. Blaszczyk, K., Nowicka, H., Kostyrko, K., Antonczyk, A., Wesoly, J., and Bluyssen, H.A.R.
650 (2016). The unique role of STAT2 in constitutive and IFN-induced transcription and antiviral
651 responses. Cytokine Growth Factor Rev. *29*, 71–81.
652 https://doi.org/10.1016/j.cytogfr.2016.02.010.

653 20. Begitt, A., Droescher, M., Meyer, T., Schmid, C.D., Baker, M., Antunes, F., Knobeloch, K.-P.,
654 Owen, M.R., Naumann, R., Decker, T., et al. (2014). STAT1-cooperative DNA binding
655 distinguishes type 1 from type 2 interferon signaling. Nat. Immunol. *15*, 168–176.
656 https://doi.org/10.1038/ni.2794.

657 21. Schoggins, J.W. (2019). Interferon-Stimulated Genes: What Do They All Do? Annu. Rev. Virol.
658 *6*, 567–584. https://doi.org/10.1146/annurev-virology-092818-015756.

659 22. Maarifi, G., Smith, N., Maillet, S., Moncorgé, O., Chamontin, C., Edouard, J., Sohm, F., Blanchet,
660 F.P., Herbeuval, J.-P., Lutfalla, G., et al. (2019). TRIM8 is required for virus-induced IFN
661 response in human plasmacytoid dendritic cells. Sci. Adv. *5*, eaax3511.
662 https://doi.org/10.1126/sciadv.aax3511.

663 23. Clay, H., Davis, J.M., Beery, D., Huttenlocher, A., Lyons, S.E., and Ramakrishnan, L. (2007).
664 Dichotomous role of the macrophage in early Mycobacterium marinum infection of the zebrafish.
665 Cell Host Microbe *2*, 29–39. https://doi.org/10.1016/j.chom.2007.06.004.

666 24. Pagán, A.J., Yang, C.-T., Cameron, J., Swaim, L.E., Ellett, F., Lieschke, G.J., and
667 Ramakrishnan, L. (2015). Myeloid Growth Factors Promote Resistance to Mycobacterial
668 Infection by Curtailing Granuloma Necrosis through Macrophage Replenishment. Cell Host
669 Microbe *18*, 15–26. https://doi.org/10.1016/j.chom.2015.06.008.

670 25. Berg, R.D., Levitte, S., O'Sullivan, M.P., O'Leary, S.M., Cambier, C.J., Cameron, J., Takaki, K.K.,
671 Moens, C.B., Tobin, D.M., Keane, J., et al. (2016). Lysosomal Disorders Drive Susceptibility to
672 Tuberculosis by Compromising Macrophage Migration. Cell *165*, 139–152.

673 https://doi.org/10.1016/j.cell.2016.02.034.

674 26. Yang, C.-T., Cambier, C.J., Davis, J.M., Hall, C.J., Crosier, P.S., and Ramakrishnan, L. (2012).
675 Neutrophils exert protection in the early tuberculous granuloma by oxidative killing of
676 mycobacteria phagocytosed from infected macrophages. Cell Host Microbe *12*, 301–312.
677 https://doi.org/10.1016/j.chom.2012.07.009.

678 27. Elks, P.M., Brizee, S., van der Vaart, M., Walmsley, S.R., van Eeden, F.J., Renshaw, S.A., and
679 Meijer, A.H. (2013). Hypoxia inducible factor signaling modulates susceptibility to mycobacterial
680 infection via a nitric oxide dependent mechanism. PLoS Pathog. *9*, e1003789.
681 https://doi.org/10.1371/journal.ppat.1003789.

682 28. Voelz, K., Gratacap, R.L., and Wheeler, R.T. (2015). A zebrafish larval model reveals early
683 tissue-specific innate immune responses to Mucor circinelloides. Dis. Model. Mech. *8*, 1375–
684 1388. https://doi.org/10.1242/dmm.019992.

685 29. Renshaw, S.A., Loynes, C.A., Trushell, D.M.I., Elworthy, S., Ingham, P.W., and Whyte, M.K.B.
686 (2006). A transgenic zebrafish model of neutrophilic inflammation. Blood *108*, 3976–3978.
687 https://doi.org/10.1182/blood-2006-05-024075.

688 30. Bucciol, G., Moens, L., Ogishi, M., Rinchai, D., Matuozzo, D., Momenilandi, M., Kerrouche, N.,
689 Cale, C.M., Treffeisen, E.R., Al Salamah, M., et al. (2023). Human inherited complete STAT2
690 deficiency underlies inflammatory viral diseases. J. Clin. Invest. *133*, e168321.
691 https://doi.org/10.1172/JCI168321.

692 31. Rauch, I., Müller, M., and Decker, T. (2013). The regulation of inflammation by interferons and
693 their STATs. JAK-STAT *2*, e23820. https://doi.org/10.4161/jkst.23820.

694 32. Gray, C., Loynes, C.A., Whyte, M.K.B., Crossman, D.C., Renshaw, S.A., and Chico, T.J.A.
695 (2011). Simultaneous intravital imaging of macrophage and neutrophil behaviour during
696 inflammation using a novel transgenic zebrafish. Thromb. Haemost. *105*, 811–819.
697 https://doi.org/10.1160/TH10-08-0525.

698 33. Ellett, F., Pase, L., Hayman, J.W., Andrianopoulos, A., and Lieschke, G.J. (2011). mpeg1
699 promoter transgenes direct macrophage-lineage expression in zebrafish. Blood *117*, e49-56.
700 https://doi.org/10.1182/blood-2010-10-314120.

701 34. Bloom, C.I., Graham, C.M., Berry, M.P.R., Wilkinson, K.A., Oni, T., Rozakeas, F., Xu, Z.,
702 Rossello-Urgell, J., Chaussabel, D., Banchereau, J., et al. (2012). Detectable Changes in The
703 Blood Transcriptome Are Present after Two Weeks of Antituberculosis Therapy. PLOS ONE *7*,
704 e46191. https://doi.org/10.1371/journal.pone.0046191.

705 35. Ottenhoff, T.H.M., Dass, R.H., Yang, N., Zhang, M.M., Wong, H.E.E., Sahiratmadja, E., Khor,
706 C.C., Alisjahbana, B., Crevel, R. van, Marzuki, S., et al. (2012). Genome-Wide Expression
707 Profiling Identifies Type 1 Interferon Response Pathways in Active Tuberculosis. PLOS ONE *7*,
708 e45839. https://doi.org/10.1371/journal.pone.0045839.

709 36. Mayer-Barber, K.D., Andrade, B.B., Barber, D.L., Hieny, S., Feng, C.G., Caspar, P., Oland, S.,
710 Gordon, S., and Sher, A. (2011). Innate and Adaptive Interferons Suppress IL-1α and IL-1β
711 Production by Distinct Pulmonary Myeloid Subsets during Mycobacterium tuberculosis Infection.
712 Immunity *35*, 1023–1034. https://doi.org/10.1016/j.immuni.2011.12.002.

713 37. Mayer-Barber, K.D., Andrade, B.B., Oland, S.D., Amaral, E.P., Barber, D.L., Gonzales, J.,
714 Derrick, S.C., Shi, R., Kumar, N.P., Wei, W., et al. (2014). Host-directed therapy of tuberculosis
715 based on interleukin-1 and type I interferon crosstalk. Nature *511*, 99–103.
716 https://doi.org/10.1038/nature13489.

717 38. Ji, D.X., Yamashiro, L.H., Chen, K.J., Mukaida, N., Kramnik, I., Darwin, K.H., and Vance, R.E.
718 (2019). Type I interferon-driven susceptibility to Mycobacterium tuberculosis is mediated by IL-
719 1Ra. Nat. Microbiol. *4*, 2128–2135. https://doi.org/10.1038/s41564-019-0578-3.

720 39. Kotov, D.I., Lee, O.V., Fattinger, S.A., Langner, C.A., Guillen, J.V., Peters, J.M., Moon, A., Burd,
721 E.M., Witt, K.C., Stetson, D.B., et al. (2023). Early cellular mechanisms of type I interferon-driven
722 susceptibility to tuberculosis. Cell *186*, 5536-5553.e22.
723 https://doi.org/10.1016/j.cell.2023.11.002.

724 40. Giosué, S., Casarini, M., Alemanno, L., Galluccio, G., Mattia, P., Pedicelli, G., Rebek, L., Bisetti,
725 A., and Ameglio, F. (1998). Effects of aerosolized interferon-alpha in patients with pulmonary
726 tuberculosis. Am. J. Respir. Crit. Care Med. *158*, 1156–1162.
727 https://doi.org/10.1164/ajrccm.158.4.9803065.

728 41. Zarogoulidis, P., Kioumis, I., Papanas, N., Manika, K., Kontakiotis, T., Papagianis, A., and
729 Zarogoulidis, K. (2012). The effect of combination IFN-alpha-2a with usual antituberculosis
730 chemotherapy in non-responding tuberculosis and diabetes mellitus: a case report and review
731 of the literature. J. Chemother. *24*, 173–177. https://doi.org/10.1179/1973947812Y.0000000005.

732 42. Mansoori, D., Tavana, S., Mirsaeidi, M., Yazdanpanah, M., and Sohrabpour, H. (2002). The
733 Efficacy of Interferon-α in the Treatment of Multidrug Resistant Tuberculosis. TANAFFOS *1*, 29–
734 34.

735 43. Liu, Y.E., Darrah, P.A., Zeppa, J.J., Kamath, M., Laboune, F., Douek, D.C., Maiello, P.,
736 Roederer, M., Flynn, J.L., Seder, R.A., et al. (2023). Blood transcriptional correlates of BCG-
737 induced protection against tuberculosis in rhesus macaques. Cell Rep. Med. *4*, 101096.
738 https://doi.org/10.1016/j.xcrm.2023.101096.

739 44. Tezera, L.B., Bielecka, M.K., Chancellor, A., Reichmann, M.T., Shammari, B.A., Brace, P., Batty,
740 A., Tocheva, A., Jogai, S., Marshall, B.G., et al. (2017). Dissection of the host-pathogen
741 interaction in human tuberculosis using a bioengineered 3-dimensional model. eLife *6*, e21283.
742 https://doi.org/10.7554/eLife.21283.

743 45. Torraca, V., Cui, C., Boland, R., Bebelman, J.-P., van der Sar, A.M., Smit, M.J., Siderius, M.,
744 Spaink, H.P., and Meijer, A.H. (2015). The CXCR3-CXCL11 signaling axis mediates
745 macrophage recruitment and dissemination of mycobacterial infection. Dis. Model. Mech. *8*,
746 253–269. https://doi.org/10.1242/dmm.017756.

747 46. Davis, J.M., Clay, H., Lewis, J.L., Ghori, N., Herbomel, P., and Ramakrishnan, L. (2002). Real-
748 time visualization of mycobacterium-macrophage interactions leading to initiation of granuloma
749 formation in zebrafish embryos. Immunity *17*, 693–702. https://doi.org/10.1016/s1074-
750 7613(02)00475-2.

751 47. Tobin, D.M., Roca, F.J., Oh, S.F., McFarland, R., Vickery, T.W., Ray, J.P., Ko, D.C., Zou, Y.,
752 Bang, N.D., Chau, T.T.H., et al. (2012). Host genotype-specific therapies can optimize the
753 inflammatory response to mycobacterial infections. Cell *148*, 434–446.
754 https://doi.org/10.1016/j.cell.2011.12.023.

755 48. Neehus, A.-L., Carey, B., Landekic, M., Panikulam, P., Deutsch, G., Ogishi, M., Arango-Franco,
756 C.A., Philippot, Q., Modaresi, M., Mohammadzadeh, I., et al. (2024). Human inherited CCR2
757 deficiency underlies progressive polycystic lung disease. Cell *187*, 390-408.e23.
758 https://doi.org/10.1016/j.cell.2023.11.036.

759 49. Walters, K.B., Green, J.M., Surfus, J.C., Yoo, S.K., and Huttenlocher, A. (2010). Live imaging of
760 neutrophil motility in a zebrafish model of WHIM syndrome. Blood *116*, 2803–2811.
761 https://doi.org/10.1182/blood-2010-03-276972.

762 50. Abel, L., Fellay, J., Haas, D.W., Schurr, E., Srikrishna, G., Urbanowski, M., Chaturvedi, N.,
763 Srinivasan, S., Johnson, D.H., and Bishai, W.R. (2018). Genetics of human susceptibility to
764 active and latent tuberculosis: present knowledge and future perspectives. Lancet Infect. Dis.
765 *18*, e64–e75. https://doi.org/10.1016/S1473-3099(17)30623-0.

766 51. Khadela, A., Chavda, V.P., Postwala, H., Shah, Y., Mistry, P., and Apostolopoulos, V. (2022).
767 Epigenetics in Tuberculosis: Immunomodulation of Host Immune Response. Vaccines *10*, 1740.
768 https://doi.org/10.3390/vaccines10101740.

769 52. Jacobs, A.L. (1941). Infective dose in pulmonary tuberculosis. Tubercle *22*, 266–271.
770 https://doi.org/10.1016/S0041-3879(41)80017-8.

771 53. Plumlee, C.R., Duffy, F.J., Gern, B.H., Delahaye, J.L., Cohen, S.B., Stoltzfus, C.R., Rustad, T.R.,
772 Hansen, S.G., Axthelm, M.K., Picker, L.J., et al. (2021). Ultra-low Dose Aerosol Infection of Mice
773 with Mycobacterium tuberculosis More Closely Models Human Tuberculosis. Cell Host Microbe
774 *29*, 68-82.e5. https://doi.org/10.1016/j.chom.2020.10.003.

775 54. Casanova, J.-L., and Anderson, M.S. Unlocking life-threatening COVID-19 through two types of
776 inborn errors of type I IFNs. J. Clin. Invest. *133*, e166283. https://doi.org/10.1172/JCI166283.

777 55. Bastard, P., Gervais, A., Le Voyer, T., Rosain, J., Philippot, Q., Manry, J., Michailidis, E.,
778 Hoffmann, H.-H., Eto, S., Garcia-Prat, M., et al. (2021). Autoantibodies neutralizing type I IFNs
779 are present in ~4% of uninfected individuals over 70 years old and account for ~20% of COVID-
780 19 deaths. Sci. Immunol. *6*, eabl4340. https://doi.org/10.1126/sciimmunol.abl4340.

781 56. Lehmann, M.H., Torres-Domínguez, L.E., Price, P.J.R., Brandmüller, C., Kirschning, C.J., and
782 Sutter, G. (2016). CCL2 expression is mediated by type I IFN receptor and recruits NK and T
783 cells to the lung during MVA infection. J. Leukoc. Biol. *99*, 1057–1064.
784 https://doi.org/10.1189/jlb.4MA0815-376RR.

785 57. Buttmann, M., Merzyn, C., and Rieckmann, P. (2004). Interferon-beta induces transient systemic
786 IP-10/CXCL10 chemokine release in patients with multiple sclerosis. J. Neuroimmunol. *156*,
787 195–203. https://doi.org/10.1016/j.jneuroim.2004.07.016.

788 58. Cambier, C.J., Takaki, K.K., Larson, R.P., Hernandez, R.E., Tobin, D.M., Urdahl, K.B., Cosma,
789 C.L., and Ramakrishnan, L. (2014). Mycobacteria manipulate macrophage recruitment through
790 coordinated use of membrane lipids. Nature *505*, 218–222. https://doi.org/10.1038/nature12799.

791 59. Elkington, P., Shiomi, T., Breen, R., Nuttall, R.K., Ugarte-Gil, C.A., Walker, N.F., Saraiva, L.,
792 Pedersen, B., Mauri, F., Lipman, M., et al. (2011). MMP-1 drives immunopathology in human
793 tuberculosis and transgenic mice. J. Clin. Invest. *121*, 1827–1833.
794 https://doi.org/10.1172/JCI45666.

795 60. Guglielmetti, L., Cazzadori, A., Conti, M., Boccafoglio, F., Vella, A., Ortolani, R., and Concia, E.
796 (2013). Lymphocyte subpopulations in active tuberculosis: association with disease severity and
797 the QFT-GIT assay. Int. J. Tuberc. Lung Dis. Off. J. Int. Union Tuberc. Lung Dis. *17*, 825–828.
798 https://doi.org/10.5588/ijtld.12.0361.

799 61. Jurado, J.O., Pasquinelli, V., Alvarez, I.B., Peña, D., Rovetta, A.I., Tateosian, N.L., Romeo, H.E.,
800 Musella, R.M., Palmero, D., Chuluyán, H.E., et al. (2012). IL-17 and IFN-γ expression in
801 lymphocytes from patients with active tuberculosis correlates with the severity of the disease. J.
802 Leukoc. Biol. *91*, 991–1002. https://doi.org/10.1189/jlb.1211619.

803 62. Hasan, Z., Jamil, B., Khan, J., Ali, R., Khan, M.A., Nasir, N., Yusuf, M.S., Jamil, S., Irfan, M., and
804 Hussain, R. (2009). Relationship between circulating levels of IFN-gamma, IL-10, CXCL9 and
805 CCL2 in pulmonary and extrapulmonary tuberculosis is dependent on disease severity. Scand.
806 J. Immunol. *69*, 259–267. https://doi.org/10.1111/j.1365-3083.2008.02217.x.

807 63. Roe, J., Venturini, C., Gupta, R.K., Gurry, C., Chain, B.M., Sun, Y., Southern, J., Jackson, C.,
808 Lipman, M.C., Miller, R.F., et al. (2020). Blood Transcriptomic Stratification of Short-term Risk in
809 Contacts of Tuberculosis. Clin. Infect. Dis. Off. Publ. Infect. Dis. Soc. Am. *70*, 731–737.
810 https://doi.org/10.1093/cid/ciz252.

811 64. Bray, N.L., Pimentel, H., Melsted, P., and Pachter, L. (2016). Near-optimal probabilistic RNA-
812 seq quantification. Nat. Biotechnol. *34*, 525–527. https://doi.org/10.1038/nbt.3519.

813 65. Soneson, C., Love, M.I., and Robinson, M.D. (2015). Differential analyses for RNA-seq:
814 transcript-level estimates improve gene-level inferences. F1000Research *4*, 1521.
815 https://doi.org/10.12688/f1000research.7563.2.

816 66. Durinck, S., Spellman, P.T., Birney, E., and Huber, W. (2009). Mapping identifiers for the
817 integration of genomic datasets with the R/Bioconductor package biomaRt. Nat. Protoc. *4*, 1184–
818 1191. https://doi.org/10.1038/nprot.2009.97.

819 67. Leek, J.T., Johnson, W.E., Parker, H.S., Jaffe, A.E., and Storey, J.D. (2012). The sva package
820 for removing batch effects and other unwanted variation in high-throughput experiments.
821 Bioinforma. Oxf. Engl. *28*, 882–883. https://doi.org/10.1093/bioinformatics/bts034.

822 68. Fang, H., Knezevic, B., Burnham, K.L., and Knight, J.C. (2016). XGR software for enhanced
823 interpretation of genomic summary data, illustrated by application to immunological traits.
824 Genome Med. *8*, 129. https://doi.org/10.1186/s13073-016-0384-y.

825 69. Turner, C.T., Brown, J., Shaw, E., Uddin, I., Tsaliki, E., Roe, J.K., Pollara, G., Sun, Y., Heather,
826 J.M., Lipman, M., et al. (2021). Persistent T Cell Repertoire Perturbation and T Cell Activation in
827 HIV After Long Term Treatment. Front. Immunol. *12*, 634489.
828 https://doi.org/10.3389/fimmu.2021.634489.

829 70. Jacomy, M., Venturini, T., Heymann, S., and Bastian, M. (2014). ForceAtlas2, a continuous
830 graph layout algorithm for handy network visualization designed for the Gephi software. PloS
831 One *9*, e98679. https://doi.org/10.1371/journal.pone.0098679.

832 71. Swindell, W.R., Xing, X., Stuart, P.E., Chen, C.S., Aphale, A., Nair, R.P., Voorhees, J.J., Elder,
833 J.T., Johnston, A., and Gudjonsson, J.E. (2012). Heterogeneity of inflammatory and cytokine
834 networks in chronic plaque psoriasis. PloS One *7*, e34594.
835 https://doi.org/10.1371/journal.pone.0034594.

836 72. Hulsen, T., de Vlieg, J., and Alkema, W. (2008). BioVenn - a web application for the comparison
837 and visualization of biological lists using area-proportional Venn diagrams. BMC Genomics *9*,
838 488. https://doi.org/10.1186/1471-2164-9-488.

839 73. Nusslein-Volhard, C. (2002). Zebrafish: A Practical Approach 1 edition. R. Dahm, ed. (Oxford
840 University Press).

841 74. Kroll, F., Powell, G.T., Ghosh, M., Gestri, G., Antinucci, P., Hearn, T.J., Tunbak, H., Lim, S.,
842 Dennis, H.W., Fernandez, J.M., et al. (2021). A simple and effective F0 knockout method for
843 rapid screening of behaviour and other complex phenotypes. eLife *10*, e59683.
844 https://doi.org/10.7554/eLife.59683.

845 75. Aggad, D., Mazel, M., Boudinot, P., Mogensen, K.E., Hamming, O.J., Hartmann, R., Kotenko,
846 S., Herbomel, P., Lutfalla, G., and Levraud, J.-P. (2009). The two groups of zebrafish virus-
847 induced interferons signal via distinct receptors with specific and shared chains. J. Immunol.
848 Baltim. Md 1950 *183*, 3924–3931. https://doi.org/10.4049/jimmunol.0901495.

849 76. Takaki, K., Davis, J.M., Winglee, K., and Ramakrishnan, L. (2013). Evaluation of the
850 pathogenesis and treatment of Mycobacterium marinum infection in zebrafish. Nat. Protoc. *8*,

1114–1124. https://doi.org/10.1038/nprot.2013.068.

77. van Leeuwen, L.M., van der Kuip, M., Youssef, S.A., de Bruin, A., Bitter, W., van Furth, A.M., and van der Sar, A.M. (2014). Modeling tuberculous meningitis in zebrafish using Mycobacterium marinum. Dis. Model. Mech. *7*, 1111–1122. https://doi.org/10.1242/dmm.015453.

78. Benard, E.L., van der Sar, A.M., Ellett, F., Lieschke, G.J., Spaink, H.P., and Meijer, A.H. (2012). Infection of zebrafish embryos with intracellular bacterial pathogens. J. Vis. Exp. JoVE. https://doi.org/10.3791/3781.

79. Wilkinson, R.N., Elworthy, S., Ingham, P.W., and van Eeden, F.J.M. (2013). A method for high-throughput PCR-based genotyping of larval zebrafish tail biopsies. BioTechniques *55*, 314–316. https://doi.org/10.2144/000114116.

80. Stirling, D.R., Suleyman, O., Gil, E., Elks, P.M., Torraca, V., Noursadeghi, M., and Tomlinson, G.S. (2020). Analysis tools to quantify dissemination of pathology in zebrafish larvae. Sci. Rep. *10*, 3149. https://doi.org/10.1038/s41598-020-59932-1.

81. Sholl, D.A. (1953). Dendritic organization in the neurons of the visual and motor cortices of the cat. J. Anat. *87*, 387–406.

82. van der Walt, S., Colbert, S.C., and Varoquaux, G. (2011). The NumPy Array: A Structure for Efficient Numerical Computation. Comput. Sci. Eng. *13*, 22–30. https://doi.org/10.1109/MCSE.2011.37.

83. van der Walt, S., Schönberger, J.L., Nunez-Iglesias, J., Boulogne, F., Warner, J.D., Yager, N., Gouillart, E., Yu, T., and scikit-image contributors (2014). scikit-image: image processing in Python. PeerJ *2*, e453. https://doi.org/10.7717/peerj.453.

84. Meeker, N.D., Hutchinson, S.A., Ho, L., and Trede, N.S. (2007). Method for isolation of PCR-ready genomic DNA from zebrafish tissues. BioTechniques *43*, 610, 612, 614. https://doi.org/10.2144/000112619.

85. Labun, K., Guo, X., Chavez, A., Church, G., Gagnon, J.A., and Valen, E. (2019). Accurate analysis of genuine CRISPR editing events with ampliCan. Genome Res. *29*, 843–847. https://doi.org/10.1101/gr.244293.118.

ACKNOWLEDGEMENTS

We thank Michelle Berin and Victoria Dean (Clinical Research Nurses, UCL Division of Infection and Immunity) and Mylah Ramirez (Research Nurse, Barts Health NHS Trust) for support with research governance, participant recruitment and sample collection. We thank the UCL Zebrafish Facility staff, particularly Heather Callaway, Jenna Hakkesteeg, Karen Dunford, Carole Wilson and Elise Hitchcock for maintenance of the zebrafish lines used in this study, especially during the first wave of the COVID-19 pandemic. We thank UCL Genomics for library preparation and sequencing of samples for transcriptional profiling (www.ucl.ac.uk/child-health/research/genetics-and-genomic-medicine/ucl-genomics). We thank Alex Lubin and Katie-Jo Miller for next generation sequencing of

888 zebrafish samples for genotyping. This work has benefited from the facilities and expertise of
889 CELPHEDIA-TEFOR, UAR2010 TEFOR Paris-Saclay (TEFOR Infrastructure - Investissement
890 d'avenir - ANR-II-INBS-0014) and from the Recombinant Protein Platform of the Institut Pasteur,
891 Paris.

892 GST is supported by a UK MRC Clinician Scientist Fellowship (MR/N007727/1). MN is supported by
893 the Wellcome Trust (207511/Z/17/Z). PME is supported by a Sir Henry Dale Fellowship jointly funded
894 by the Wellcome Trust and the Royal Society (105570/Z/14/Z). J-PL is supported by Fondation pour
895 la Recherche Medicale (grant EQU202203014646). MN and GST are also supported by NIHR
896 Biomedical Research Centre Funding to University College Hospitals NHS Foundation Trust and
897 University College London.

898 **AUTHOR CONTRIBUTIONS**

899 Conceived the study: GST, MN

900 Collected the data: ASS, BSMDDE, JR, AC, ET, GP, J-PL, GST

901 Provided resources or analysis tools: ASS, BSMDDE, JR, CTT, MCIL, HK, GP, PME, EMP, J-PL,
902 MN, GST

903 Performed the data analysis / interpretation: ASS, BSMDDE, JR, CTT, GP, PME, EMP, J-PL, MN,
904 GST

905 Prepared the manuscript draft: GST, ASS, BSMDDE

906 All authors reviewed and contributed to the final manuscript.

907 **COMPETING INTERESTS**

908 The authors declare no competing interests.

909 **DATA AVAILABILITY**

910 Human TST RNAseq data and peripheral blood RNAseq data from healthy individuals are already
911 available in the ArrayExpress repository under accession numbers E-MTAB-6816 and E-MTAB-
912 10022, respectively. Human peripheral blood data from TB patients and zebrafish RNAseq data will
913 be made available in ArrayExpress at the time of peer reviewed publication of the manuscript. Source

914 data for figure panels with fewer than 20 data points are available in Data S1.

915 **CODE AVAILABILITY**

916 The source code and manual for QuantiFish software used for analysis of bacterial burden and
917 dissemination in zebrafish larvae are available at https://github.com/DavidStirling/QuantiFish. The
918 ImageJ macro used to generate montages from the Hermes images and source code and manual
919 for the Python script used for analysis of steady state cell numbers and cellular recruitment in
920 zebrafish are available at https://github.com/AndSzyShe/particle_analysis.

921

922 **FIGURES**

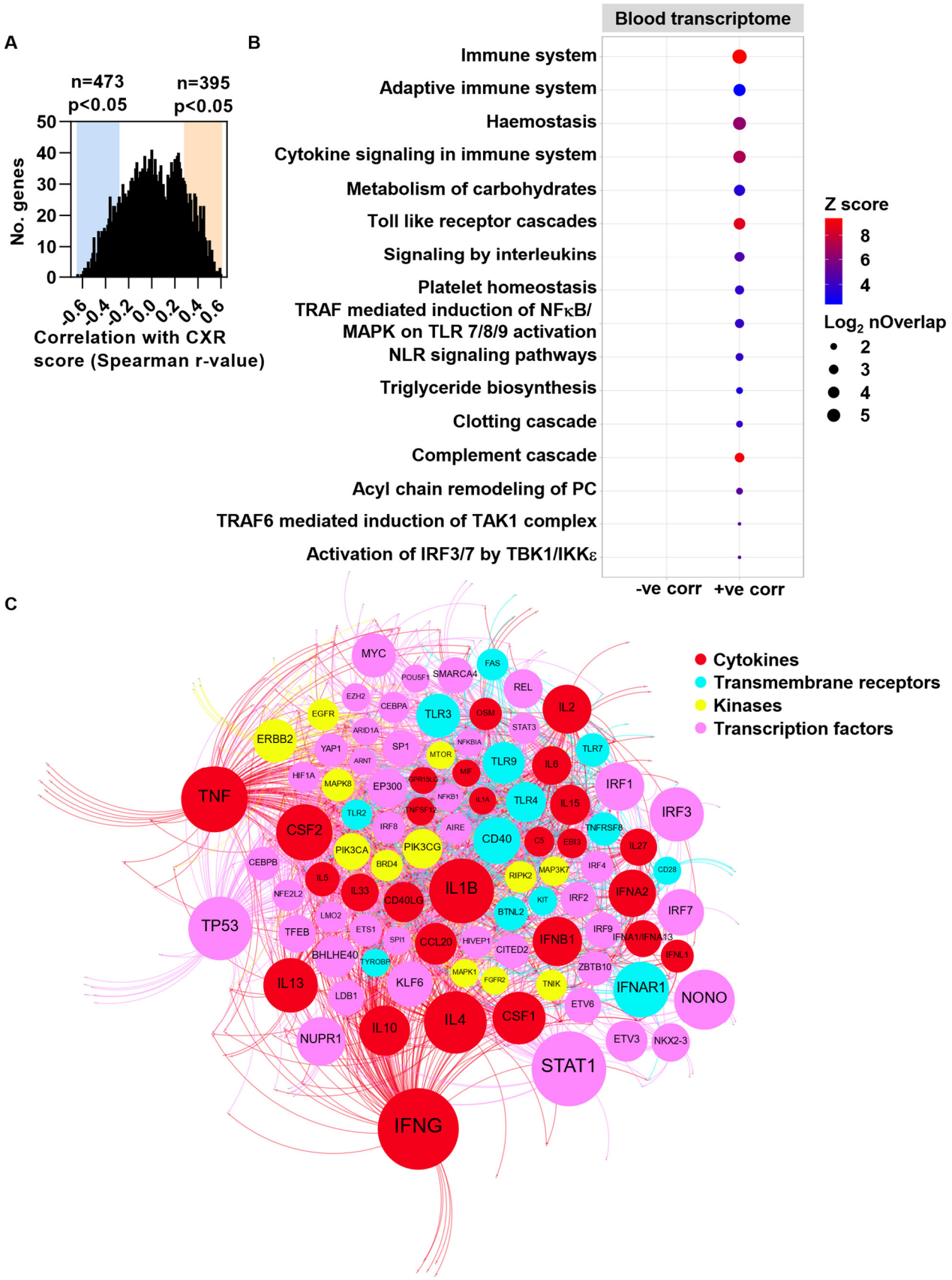

923

924 **Figure 1. The steady state human peripheral blood transcriptome reflects immune responses**

925 **positively correlated with TB severity. (A)** Frequency distribution of the correlation coefficients for
926 the relationship between the abundance of each of the 2620 transcripts which define the peripheral
927 blood transcriptome derived from 50 individuals with pulmonary tuberculosis (TB) and radiographic
928 disease severity. Coloured boxes highlight statistically significant correlations ($p<0.05$).
929 **(B)** Reactome pathway enrichment among blood transcriptome genes whose expression is
930 statistically significantly correlated with radiographic TB disease severity; corr = correlated.
931 **(C)** Network diagram of statistically significant (FDR<0.05) upstream regulators (labelled nodes)
932 coloured by their molecular function, of target gene modules whose expression is positively
933 correlated with radiological TB severity. Size of the nodes for upstream regulators is proportional to
934 -Log10 adjusted p value. Nodes were clustered using the Force Atlas 2 algorithm in Gephi (version
935 0.9.2).

936

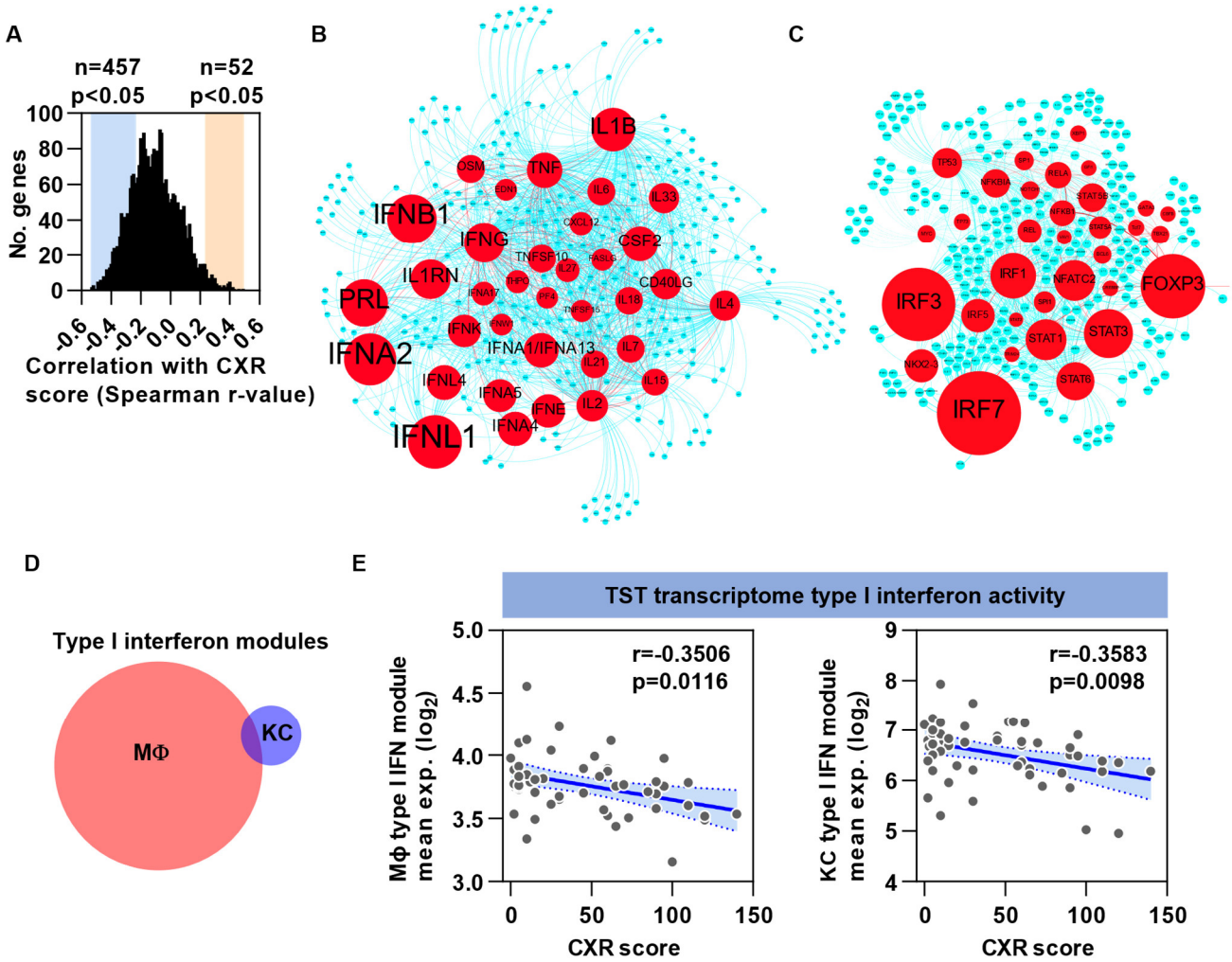

Figure 2. Reduced type I interferon activity in the TST transcriptome is associated with increased severity of human pulmonary TB disease. (A) Frequency distribution of the correlation coefficients for the relationship between the abundance of each of the 3222 transcripts within the TST transcriptome derived from 51 individuals with pulmonary TB and radiographic disease severity. Coloured boxes highlight statistically significant correlations ($p<0.05$). **(B, C)** Network diagrams of statistically significant (FDR<0.05) cytokines **(B)** and transcription factors **(C)** predicted to be upstream regulators (red) of target gene (blue) modules whose expression is negatively correlated with radiological TB severity. Size of the nodes for upstream regulators is proportional to -Log10 adjusted p value. Nodes were clustered using the Force Atlas 2 algorithm in Gephi (version 0.9.2). **(D, E)** The inverse relationship between average expression in each TST sample of two distinct, independently derived gene modules specific for type I interferon activity (Table S1) **(D)** with TB severity **(E)**. r values and p values were derived from two-tailed Spearman rank correlations. CXR = Chest x-ray, MΦ = Macrophage, KC = Keratinocyte.

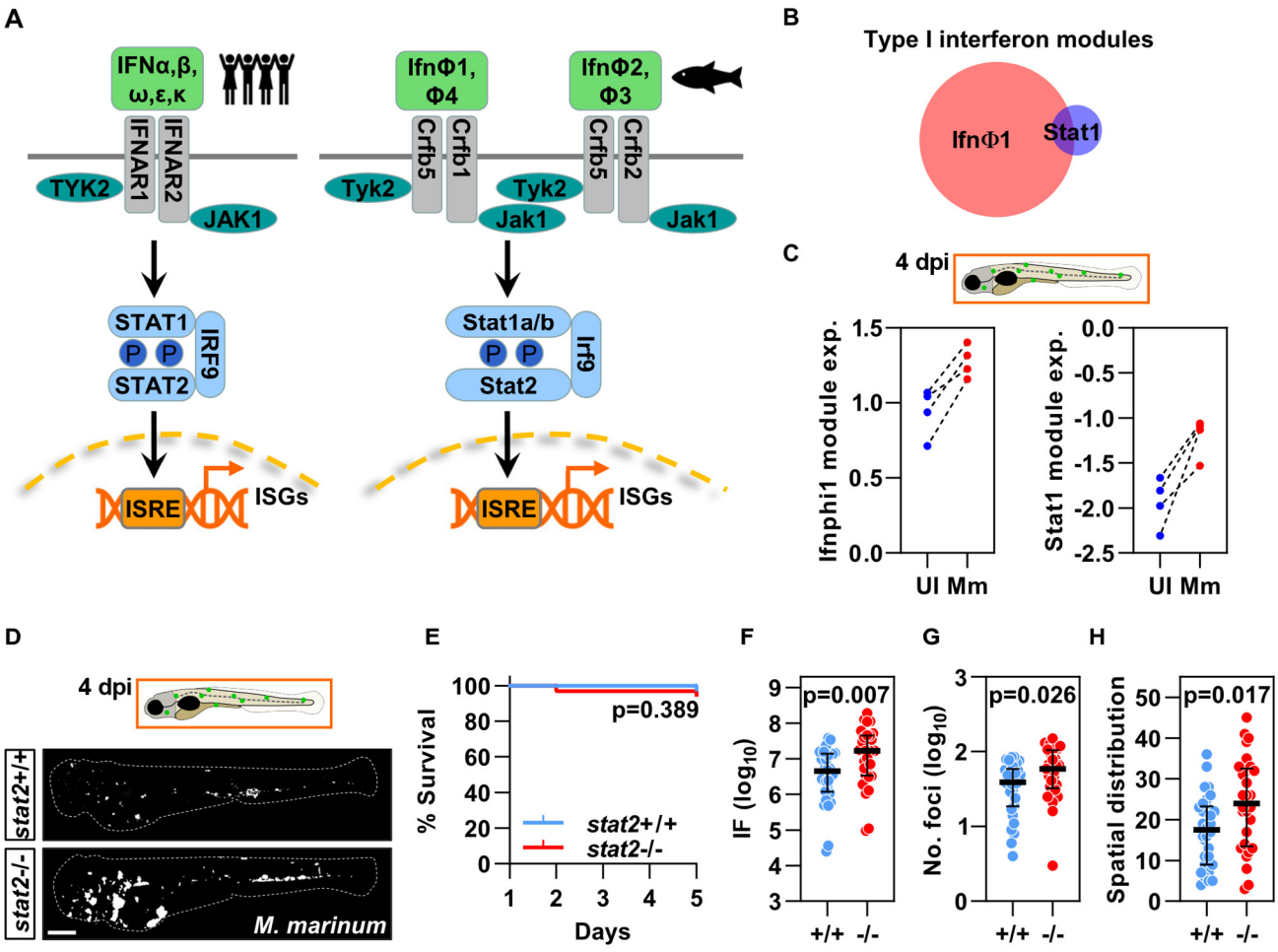

Figure 3 Increased severity of *M. marinum* infection in *stat2* CRISPants. (A) Schematic representation of the human canonical type I interferon signalling pathway (left) which is highly conserved in zebrafish (right). **(B, C)** The average expression of two largely non-overlapping **(B)** type I interferon inducible gene modules derived from independent data (Table S1) in genome-wide mRNA sequencing data from whole wild type embryos four days post-intravenous infection with 400 colony forming units (cfu) of *M. marinum* (Mm) compared with uninfected (UI) siblings **(C)**. Data are from four independent experiments. **(D)** *stat2* CRISPant (*stat2*-/-) and control ribonucleoprotein (RNP) injected (*stat2*+/+) zebrafish larvae four days post intravenous infection with 400 cfu *M. marinum*. Scale bar = 250 µm. Dashed white lines indicate the outline of each larva. **(E)** Survival of control and *stat2* disrupted zebrafish larvae 1-4 days post infection with *M. marinum*. p value was derived from a log-rank (Mantel-Cox) test. **(F-H)** Comparison of integrated fluorescence (IF) (a surrogate for bacterial burden) **(F)**, number of bacterial foci **(G)** and spatial distribution of bacteria **(H)**, in *stat2* CRISPants compared to control RNP injected siblings. Each data point represents an

individual zebrafish larva, lines and error bars indicate the median and interquartile range. p values were derived from two-tailed Mann-Whitney tests. Data are representative of four experiments. dpi = days post-infection.

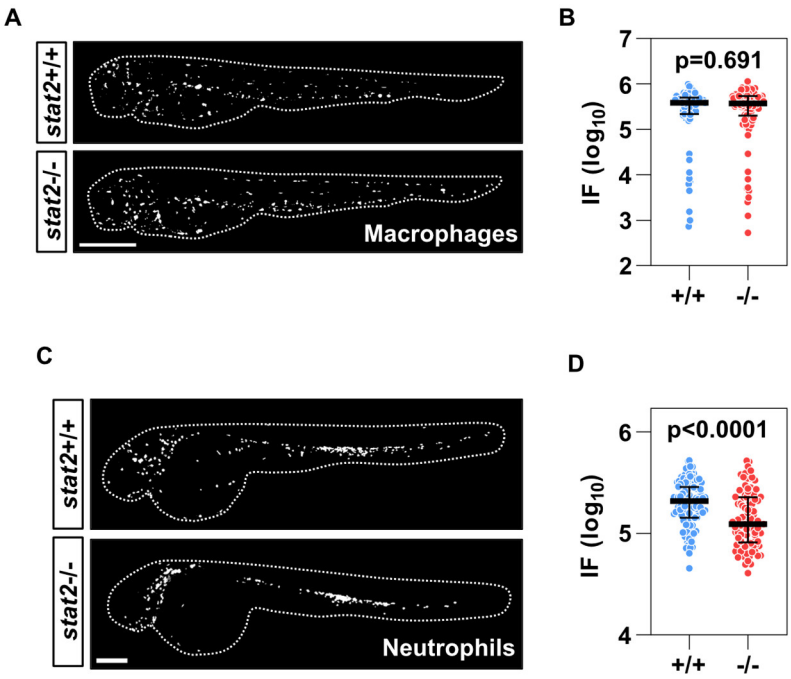

Figure. 4. Reduced steady state neutrophil numbers in *stat2* CRISPants. (A) Representative images of three day post-fertilisation (dpf) control (upper panel) and *stat2* CRISPant (lower panel) *Tg(mpeg1:mCherry)* zebrafish larvae delineated by the dashed white lines. Scale bar = 250 µm. **(B)** Integrated fluorescence (IF) as a surrogate for steady state macrophage numbers in three dpf *stat2* CRISPants compared to siblings injected with scrambled ribonucleoproteins (RNPs). **(C)** Representative images of two dpf control (upper panel) and *stat2* CRISPant (lower panel) *Tg(mpx:eGFP)* zebrafish larvae delineated by the dashed white lines. Scale bar = 250 µm. **(D)** Quantitation of baseline neutrophil numbers (represented by IF) in two dpf *stat2* CRISPants and negative control RNP injected siblings. Each data point represents an individual zebrafish larva, lines and error bars indicate the median and interquartile range. p values were derived from two-tailed Mann-Whitney tests. Data are from three independent experiments.

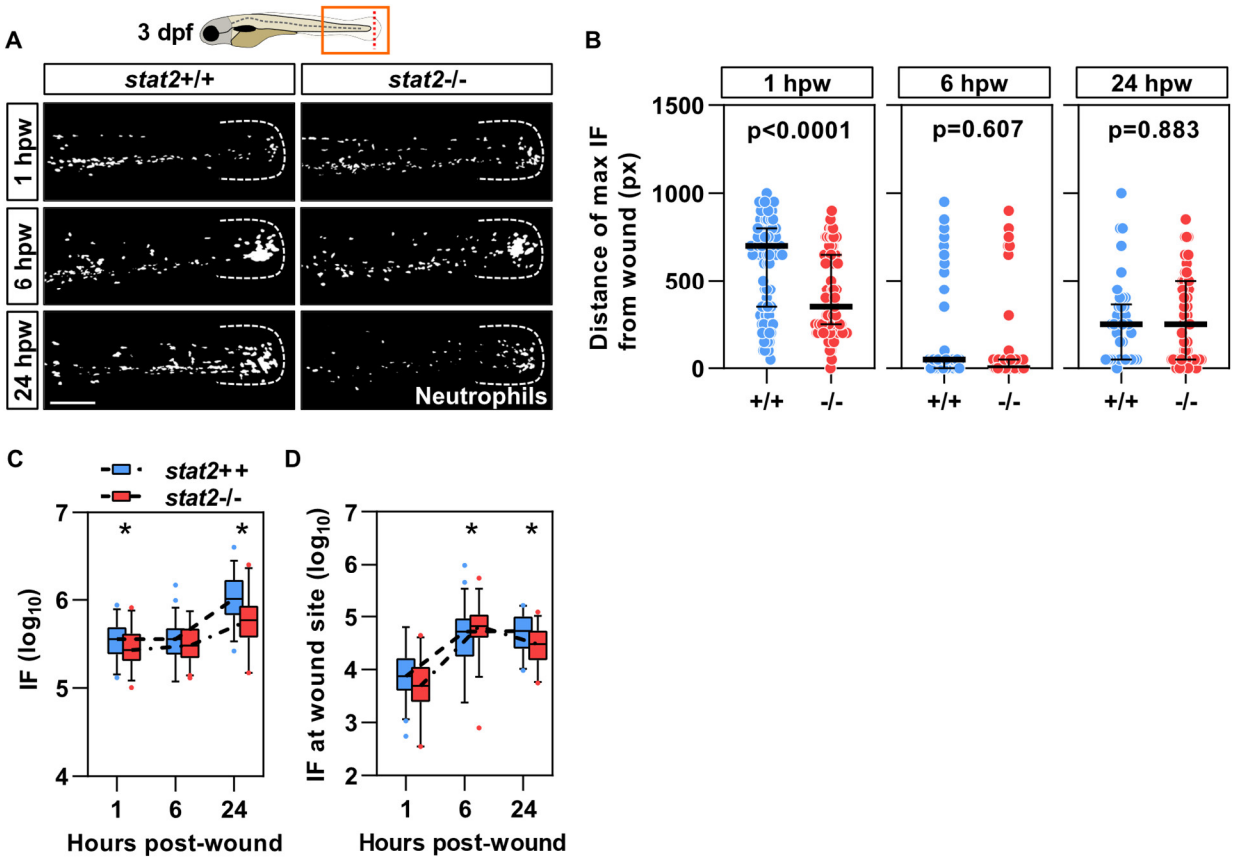

982

983 **Figure. 5. Neutrophil recruitment to the site of sterile injury is not *stat2* dependent.**
984 **(A)** Representative images of eGFP-expressing neutrophils recruited to the site of injury 1, 6 and 24
985 hours following tailfin transection of three day post-fertilisation (dpf) *stat2* CRISPant *Tg(mpx:eGFP)*
986 zebrafish larvae and scrambled ribonucleoprotein (RNP) injected controls. Scale bar represents
987 100 µm. The white dashes indicate the outline of the tailfin. **(B)** Distance of neutrophils from the
988 injury site at 1, 6 and 24 hours post-wound (hpw), derived by identifying the Sholl circle in which the
989 maximum integrated fluorescence (IF), a surrogate for highest cell numbers, was detected in *stat2*
990 CRISPants and scrambled RNP injected siblings. **(C-D)** IF, a surrogate for total neutrophil numbers
991 **(C)**, and IF at the wound site, representing neutrophil numbers localized to the tailfin transection **(D)**
992 are shown at 1, 6 and 24 hours following injury. On scatter plots data points represent individual
993 zebrafish larvae and lines and error bars the median and interquartile range. On box and whisker
994 plots horizontal lines represent median values, box limits indicate the interquartile range and
995 whiskers extend between the 5th and 95th percentiles. p values were derived from two-tailed Mann-
996 Whitney tests. * = $p<0.05$. Data are from three independent experiments. px = Pixels.

997

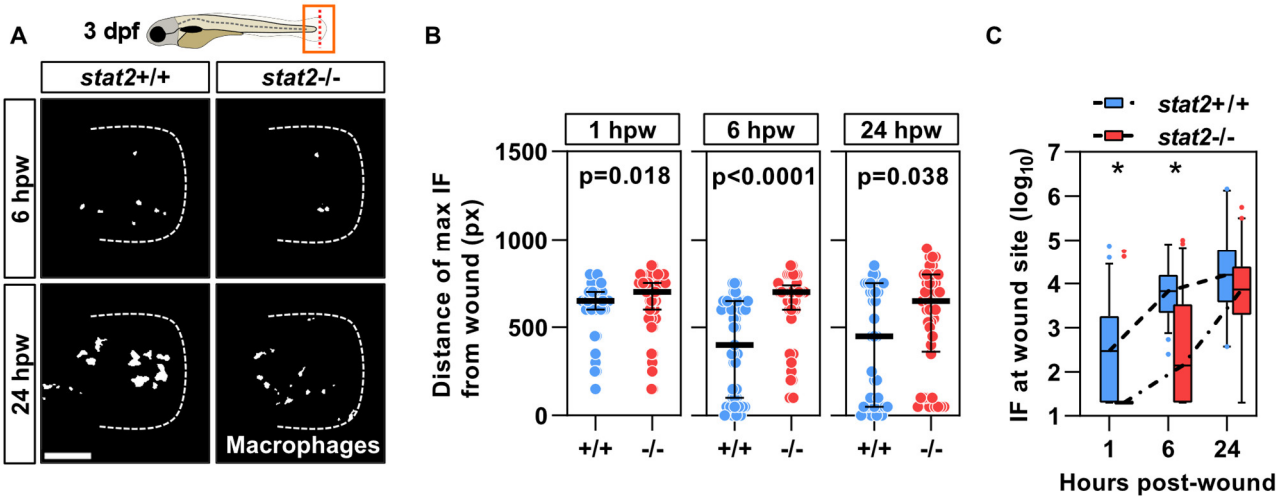

998

999 **Figure. 6. Reduced macrophage recruitment to the site of sterile injury in *stat2* CRISPants.**
1000 **(A)** Representative images of mCherry-expressing macrophages recruited to the site of tailfin
1001 transection by 6 and 24 hours, in three day post-fertilisation (dpf) *stat2* CRISPant
1002 *Tg(mpeg1:mCherry)* zebrafish embryos and controls. Scale bar represents 100 µm. The dashed
1003 white lines indicate the edge of the tailfin. **(B)** Comparison of the distance of macrophages from the
1004 site of injury at the indicated time points for *stat2* CRISPants and control RNP injected siblings. **(C)**
1005 Integrated fluorescence (IF) a surrogate for macrophage numbers at the site of tailfin transection is
1006 shown at 1, 6 and 24 hours post-wound (hpw). On scatter plots data points represent individual
1007 zebrafish larvae and lines and error bars the median and interquartile range. On box and whisker
1008 plots horizontal lines represent median values, box limits indicate the interquartile range and
1009 whiskers extend between the 5th and 95th percentiles. p values were derived from two-tailed Mann-
1010 Whitney tests. * = $p<0.05$. Data are from three independent experiments. px = Pixels.

1011

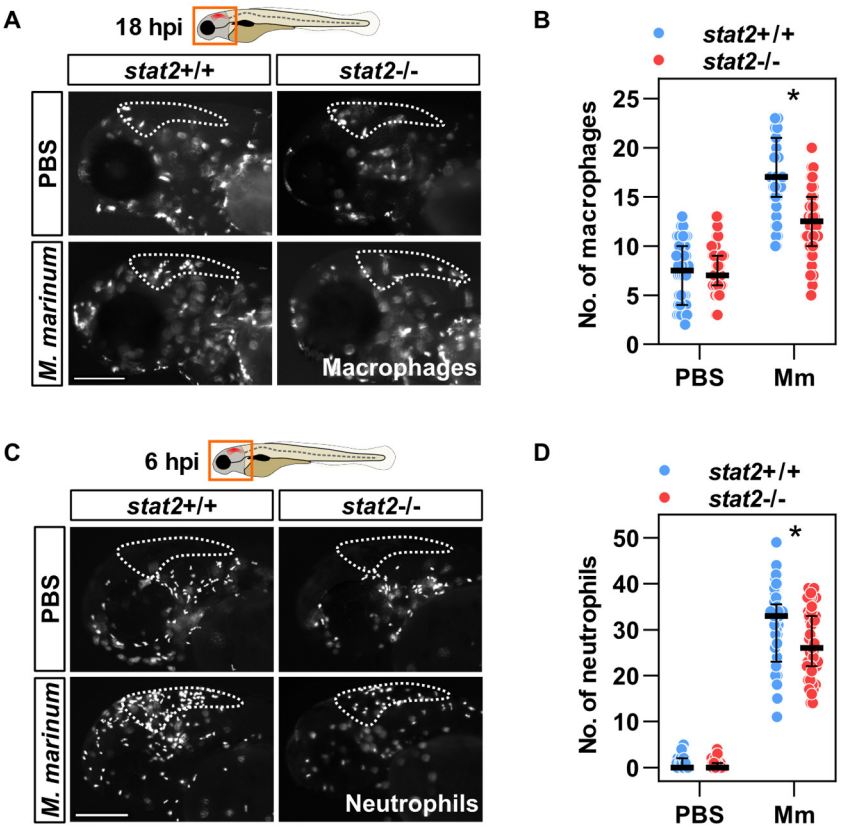

Figure. 7. Reduced macrophage and neutrophil recruitment to *M. marinum* in *stat2* CRISPants. (A) Representative images of mCherry-expressing macrophages recruited to the hindbrain (dashed white outline) 18 hours post-injection (hpi) of PBS or 200 colony forming units (cfu) *M. marinum* in two day post-fertilisation (dpf) *stat2* CRISPant *Tg(mpeg1:mCherry)* zebrafish larvae and scrambled ribonucleoprotein (RNP) injected controls. **(B)** Number of macrophages recruited to the hindbrain in response to PBS or *M. marinum* in *stat2* CRISPants and negative control RNP injected siblings. **(C)** Representative images of eGFP-expressing neutrophils recruited to the hindbrain (dashed white outline) 6 hours after PBS or *M. marinum* injection (200 cfu) in two dpf *stat2* CRISPant and control *Tg(mpx:eGFP)* zebrafish larvae. **(D)** Quantitation of neutrophils recruited to the site of *M. marinum* infection in *stat2* CRISPants and control siblings. Scale bars represent 100 µm. Data points represent individual zebrafish larvae and lines and error bars the median and interquartile range. p values were derived from two-tailed Mann-Whitney tests. * = $p<0.05$. Data are from three independent experiments.

1027 **TABLES**

		TST*	Saline controls	Blood controls
Number		51	49	58
Age	(median and range)	30 (19-77)	28 (18-75)	36 (21-69)
Sex	Male	31 (61%)	19 (39%)	16 (28%)
	Female	20 (39%)	30 (61%)	42 (72%)
Ethnicity	White	21 (41%)	20 (41%)	44 (76%)
	Asian	15 (29%)	8 (16%)	9 (15%)
	Black	12 (24%)	7 (14%)	1 (2%)
	Mixed	2 (4%)	1 (2%)	4 (7%)
	South American	1 (2%)	11 (22%)	0
	Not recorded	0	2 (4%)	0
Intradermal injection site induration (mm)	(median and range)	20 (0-70)	0	NA
Days TB treatment before TST +/ saline	(median and range)	19 (0-30)	15 (0-28)**	NA
CXR severity score	(median and range)	30 (0-140)	15 (0-110)**	NA

1028

1029 **Table 1. Clinical and demographic data summary.** Demographic characteristics and magnitude
1030 of clinical induration of the skin at the site of TST or saline injection are summarised for all study
1031 subjects. Duration of anti-tuberculous drug treatment at the time of sampling and radiographic
1032 disease severity data are provided for individuals with pulmonary TB. *Peripheral blood samples
1033 were also taken from 50 of these individuals with pulmonary TB. Saline samples were obtained from
1034 17 individuals with pulmonary TB and 32 healthy participants who were people with cured or latent
1035 TB, BCG vaccine recipients and healthy volunteers, described previously [10]. Control blood samples
1036 from healthy individuals were described previously [13]. **Applies only to participants with active TB
1037 receiving saline injections. CXR = chest x-ray.